Shallow slab fluid release across and along the Mariana arc-basin system: Insights from geochemistry of serpentinized peridotites from the Mariana fore arc

Ivan P. Savov,[1] Jeffrey G. Ryan,[2] Massimo D'Antonio,[3] and Patricia Fryer[4]

Received 12 September 2006; revised 20 April 2007; accepted 14 June 2007; published 27 September 2007.

[1] Shallow slab devolatilization is not only witnessed through fluid expulsion at accretionary prisms, but is also evidenced by active serpentinite seamounts in the shallow fore-arc region of the Mariana convergent margin. Ocean Drilling Program (ODP) Leg 195 recovered serpentinized peridotites that present a unique opportunity to study the products of shallow level exchanges between the upper mantle and slab-derived fluids. Similar to samples recovered during ODP Leg 125, the protoliths of these fore-arc serpentinized peridotites are mantle harzburgites that have suffered large volume melt extraction (up to 25%) prior to interactions with fluids released from the downgoing Pacific Plate. Samples recovered from both ODP legs 125 and 195 show U-shaped rare earth element (REE) patterns and very low REE abundances (0.001–0.1 $\times$ chondrites). Relative to global depleted mantle values these rocks typically have 1–2 orders of magnitude lower high field strength elements, REE, Th, and U contents. Interestingly, all fore-arc rocks thus far examined show extreme enrichments of fluid mobile elements (FME: B, As, Cs, Sb, Li). Because the elemental and B, Li, and Sr isotope systematics in these fore-arc serpentinites point to nonseawater-related processes, studies of elemental excesses and anomalous isotopic signatures allow assessment of how much of the subducted inventory is lost during the initial subduction process between 10 and 40 km. On the basis of similar but substantial enrichments of FME in the Mariana fore-arc samples recovered at ODP legs 125 and 195, we report large slab inventory depletions of B ($\sim$75%), Cs ($\sim$25%), As ($\sim$15%), Li ($\sim$15%), and Sb ($\sim$8%); surprisingly low (generally less than 2%) depletions of Rb, Ba, Pb, U, Sr; and no depletions in REE and the high field strength elements (HFSE). Such slab-metasomatized mantle wedge materials may be dragged to depths of arc magma generation, as proposed by Tatsumi (1986) and Straub and Layne (2002) and thus represent an unexplored class of mantle material, different in its origins, physical properties and geochemical fingerprint from mantle rocks traditionally used in modeling a wide range of subduction zone processes.

Citation: Savov, I. P., J. G. Ryan, M. D'Antonio, and P. Fryer (2007), Shallow slab fluid release across and along the Mariana arc-basin system: Insights from geochemistry of serpentinized peridotites from the Mariana fore arc, *J. Geophys. Res.*, *112*, B09205, doi:10.1029/2006JB004749.

1. Introduction

[2] Recent advances in the studies of subduction zones have stressed the importance of the subarc mantle for creating the distinct signatures that island arc lavas possess [*Carmichael et al.*, 1996; *Kepezhinskas et al.*, 1996; *Peate and Pearce*, 1998; *Parkinson and Arculus*, 1999; *Pearce et al.*, 1999, 2000; *Straub and Layne*, 2002; *Kelemen et al.*, 2003; *Morris and Ryan*, 2003; *Leeman et al.*, 2005; *Stern et al.*, 2004, 2006]. These studies almost exclusively use inferred upper mantle compositions based on data for modern residual peridotites and their derivatives from oceanic settings (mid-ocean ridges and ocean islands [*Bonatti et al.*, 1984; *Niu and Hékinian*, 1997; *Hochstaedter et al.*, 2001; *Walter*, 2003; *Kelley et al.*, 2003; *Staudigel*, 2003]) or orogenic settings (ophiolites and ultramafic massifs [*Sharma and Wasserburg*, 1996; *Gruau et al.*, 1998; *Walter*, 2003; *Bodinier and Godard*, 2003]). Data for arc-related mantle compositions, from arc mantle xenoliths and like sources, have become available only relatively recently, and from only a few subduction settings (i.e., Cascades arc [*Ertan and Leeman*, 1999; *Parkinson and Arculus*, 1999];

[1]Department of Terrestrial Magnetism, Carnegie Institution of Washington, Washington, D. C., USA.
[2]Geology Department, University of South Florida, Tampa, Florida, USA.
[3]Dipartimento di Scienze della Terra, Università degli Studi di Napoli Federico II, and Istituto Nazionale di Geofisica e Vulcanologia, Osservatorio Vesuviano, Naples, Italy.
[4]Hawai'i Institute of Geophysics and Planetology, University of Hawaii at Manoa, Honolulu, Hawaii, USA.

0148-0227/07/2006JB004749$09.00

Kamchatka arc [*Kepezhinskas et al.*, 1996; *Halama et al.*, 2006]; Mexican Volcanic Belt [*Luhr and Aranda-Gómez*, 1997]; Philippine island arc [*Maury et al.*, 1992]; South Sandwich island arc [*Pearce et al.*, 2000]; the Talkeetna arc intrusive sequences [*Kelemen et al.*, 2003]; Solomons, Vanuatu and Lesser Antilles (Grenada) island arcs [*Parkinson and Arculus*, 1999; *Parkinson et al.*, 2004]). Given the diverse conditions of their eruption/emplacement, these ultramafic samples may or may not accurately reflect the mineralogy and chemical signatures of the mantle wedge beneath arcs.

[3] A challenge in assessing the chemical character of the mantle wedge is the fact that it necessarily changes as a function of progressive chemical inputs from the downgoing slab [see *Plank and Langmuir*, 1993; *Kepezhinskas et al.*, 1996; *Schmidt and Poli*, 1998, 2003]. Changes in subarc mantle composition can be indirectly tracked through the changes in arc magma compositions observed across and along arcs [e.g., *Ryan et al.*, 1995, 1996; *Hochstaedter et al.*, 2001], but connecting changes in lava composition to mantle chemistry is complicated by variations in the melting, crystallization and assimilation processes that arc magmas undergo from source to surface. Access to mantle samples that have been impacted by slab input processes provides a baseline composition against which subarc mantle rocks and arc lavas can be compared to assess the chemical changes related to material releases from the downgoing slab.

[4] The Mariana fore arc lies at the eastern edge of the nonaccretionary convergent margin between the Mariana Trench and the Mariana volcanic arc (Figure 1) [*Mrosowski et al.*, 1981; *Fryer et al.*, 1992; *Stern et al.*, 2004]. Serpentinite mud volcanism has formed large edifices (up to 50 km in diameter and 2 km high) in the eastern half of the fore arc (Figure 2). Samples from the shallow (~30 km) Mariana fore-arc mantle were recovered during ODP Leg 125, and during Leg 195 at Site 1200 [*Fryer et al.*, 1992; *Fryer and Salisbury*, 2006]. These serpentinized peridotites represent upper mantle rocks modified by slab-derived fluids from the actively subducting Pacific Plate [*Mottl et al.*, 2003; *Fryer and Salisbury*, 2006] and provide us with an opportunity to assess the importance of shallow devolatilization processes within an active subduction zone.

[5] The samples recovered by ODP Leg 195 were "exhumed" (emplaced) onto the seafloor by rising serpentine muds that enclose blocks of hard rock "xenoliths" or clasts of serpentinized fore-arc mantle rocks (sometimes several meters in diameter). South Chamorro Seamount is one of roughly 20 large serpentinite mud volcanoes discovered so far in the Mariana fore-arc region [*Fryer et al.*, 1992, 1999, 2006; *Fryer and Salisbury*, 2006] (Figure 1). In 1990, ODP Leg 125 penetrated serpentinized peridotite samples at Conical Seamount, almost 1000 km to the north of Site 1200 (Figure 1). The lithology, metamorphic conditions and bulk rock and fluid geochemistry of ODP Leg 125 are now well described in the geologic literature [*Fryer et al.*, 1992, 1999; *Mottl*, 1992; *Parkinson et al.*, 1992; *Parkinson and Pearce*, 1998; *Savov et al.*, 2005a, 2005b]. On the basis of earthquake locations and knowledge of the dip of the subducting Pacific slab, the estimated depth to slab under the South Chamorro and Conical seamounts is ~30 km. Thus any geochemical differences between the mineralogically similar rock suites recovered from these two seamounts may reflect variations in shallow devolatilization outfluxes along the Marianas fore arc, due possibly to changes in trench inputs [*Plank and Langmuir*, 1998; *Kelley et al.*, 2003].

[6] In this paper we present whole rock major and trace element contents, and Sr isotope ratios for serpentinized ultramafic clasts from South Chamorro Seamount. This study will allow us to constrain the average composition of serpentinized fore-arc mantle directly overlying the subducting slab. We will also suggest a relative order of elemental fluid mobilities. Our results confirm and quantify the role that serpentinized mantle plays in the supply of fluids and some elements which must be added to the mantle wedge for arc magmatism to occur [*Tatsumi*, 1986; *Tatsumi and Eggins*, 1995; *Straub and Layne*, 2002; *Schmidt and Poli*, 2003; *Leeman et al.*, 2005; *Stern et al.*, 2006].

2. Geological Setting

[7] The Izu-Bonin-Mariana (IBM) arc system extends for ~2800 km, from near Tokyo (Japan) to south of Guam (Mariana Islands), where the Mesozoic Pacific Plate is being subducted west-northwestward beneath the West Philippine Plate (Figure 1). The Pacific Plate descends at a 20° dip angle to a depth of ~60 km, while at depths >100 km it sinks abruptly (almost vertically in the Mariana segment, and ~65° in the Izu-Bonin segment) beneath the West Philippine Plate [*Fryer et al.*, 1992; *Stern et al.*, 2004]. The nature of dredged samples from the slopes of the Mariana Trench (i.e., island arc tholeiites and boninites) suggests little or no sediment accretion, and that little or no oceanic crust is currently underplating in the Marianas margin [*Dietrich et al.*, 1978; *Beccaluva et al.*, 1980; *Mrosowski et al.*, 1981; *Bloomer*, 1983; *Fryer et al.*, 1992; *Plank and Langmuir*, 1998; *Stern et al.*, 2004].

[8] The Mariana fore-arc region has responded to collisions with large oceanic plateaus (similar to the Ogasawara Plateau) via vertical tectonism [*Fryer and Fryer*, 1987; *Fryer et al.*, 1995]. The resulting high abundance of faults in the outer fore arc is well documented by the Deep Sea Drilling Project (DSDP) Leg 60 (sites 458 and 459) [*Hussong et al.*, 1981]. Regional seafloor mapping [*Fryer and Fryer*, 1987; *Wessel et al.*, 1994; *Fryer et al.*, 1995; *Stern et al.*, 2004] and multichannel seismic surveys [*Mrosowski et al.*, 1981; *Fryer*, 2002; *Fryer et al.*, 2006] also confirm that faulting is pervasive in the outer half of the fore arc. Serpentinite seamounts in the Mariana fore arc occur in a zone roughly 100 km wide, on the eastern edge of the fore arc. More than 20 serpentine seamounts (mud volcanoes) have been documented within 120 km of the trench axis [*Fryer et al.*, 1995, 1999, 2006] (Figure 1). The edifices occur either at the intersection of two fault trends, or along the edges of horst blocks [*Fryer et al.*, 2000; *Fryer*, 2002].

[9] The serpentine seamounts are conical in shape, 10–50 km in diameter at their bases, and 500–2000 m high [*Fryer et al.*, 1985, 2000, 2006; *Ishii et al.*, 1992] (Figure 2). South Chamorro Seamount is considered active because of the discovery of recent mud extrusions (mudflows) and the documented venting of fresh cold fluids [*Mottl et al.*, 2003;

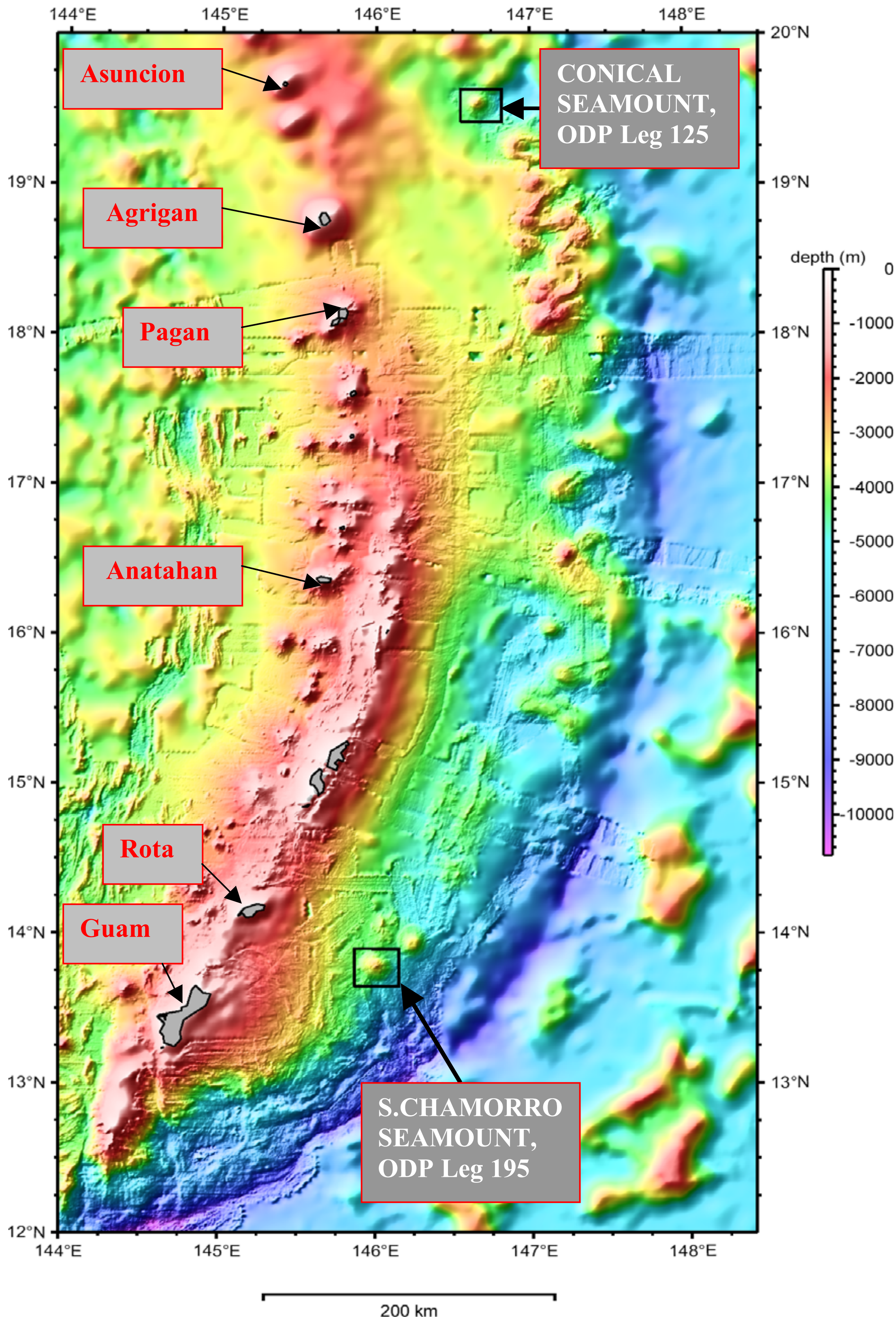

Figure 1. Bathymetry map of the Mariana arc-basin system showing the location of South Chamorro Seamount (Leg 195) and Conical Seamount (Leg 125) in relation to the volcanic islands of (from south to north) Guam, Rota, Anatahan, Pagan, Agrigan, and Asuncion. Note that the distance between the ODP Leg 125 and Leg 195 drill sites is almost 1000 km and that ~50 km to the south of South Chamorro Seamount the water depths exceed 8 km.

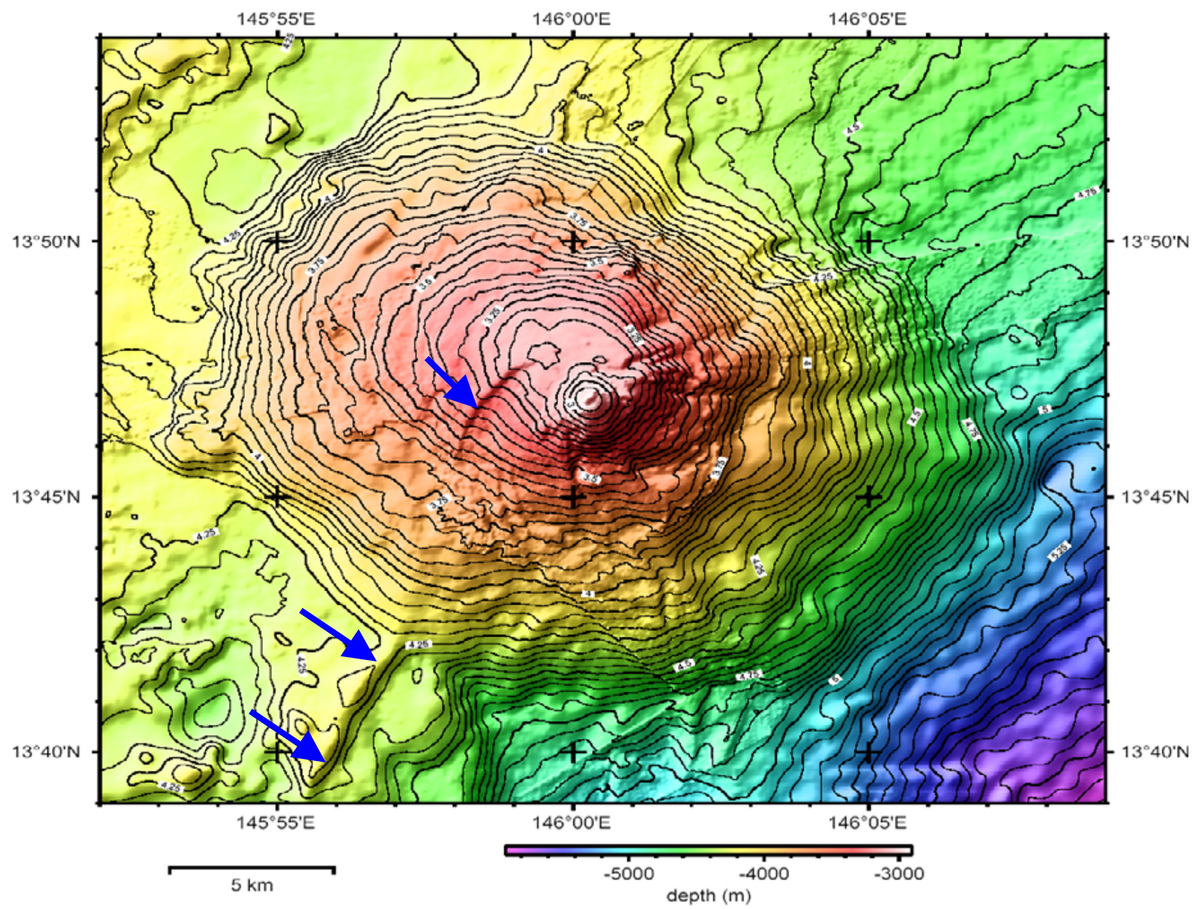
145°55'E
146°00'E
146°05'E
13°50'N
13°45'N
13°40'N
5 km
-5000
-4000
-3000
depth (m)

A

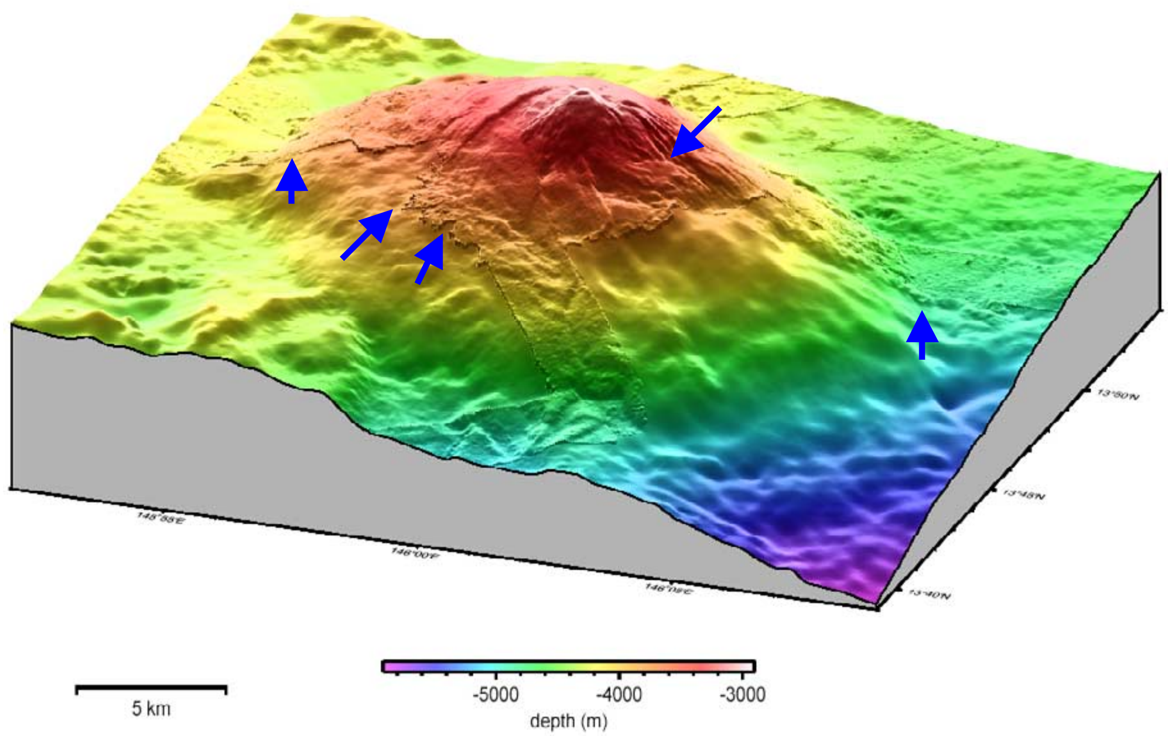
5 km
-5000
-4000
-3000
depth (m)

B

Figure 2

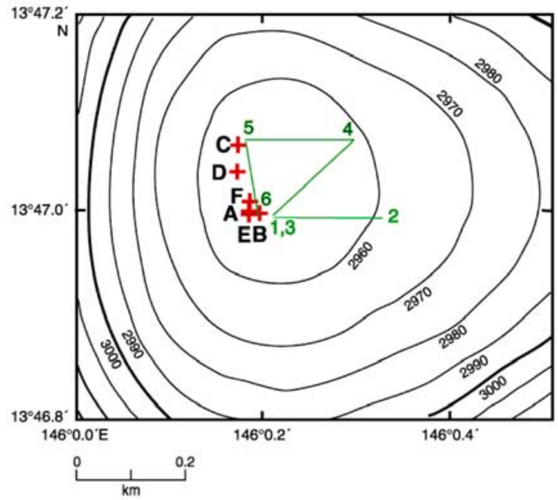

Figure 3. Summit site of the South Chamorro Seamount with the location of ODP Site 1200, holes A through F. Also shown are R/V *JOIDES Resolution* camera survey tracks (marked 1 through 6) [from *Salisbury et al.*, 2002].

Fryer and Salisbury, 2006; *Fryer et al.*, 2006]. The geochemistry of pore waters collected at these seamounts indicates deep slab origins [*Mottl*, 1992; *Fryer et al.*, 1999; *Mottl et al.*, 2003].

3. Sample Selection

[10] The samples discussed in this paper were selected from drill cores recovered at the South Chamorro Seamount during ODP Leg 195, at Site 1200 (Figures 1 and 2). Several holes (A through F) were drilled on a 200-m-high tumescent knoll at the summit (Figure 3). The drill sites are located at 13°47′N, 146°00′E, at a water depth of 2930 m below seafloor (mbsf), ~125 km east of Guam in the western Pacific Ocean (Figure 1). South Chamorro Seamount lies ~85 km from the Mariana Trench, and the estimated depth to the subducting Pacific oceanic crust beneath the seamount is ~27 km. Cold fluids with extremely high pH (~12.5) are currently seeping from aragonite and brucite chimneys. Pore waters were collected from serpentinite mud samples obtained by gravity coring [*Fryer et al.*, 1999, 2006] and by ODP Leg 195 piston core drilling [*Salisbury et al.*, 2002; *Fryer et al.*, 2006]. The pore fluid geochemistry reveals a component in the source of the fluids that could only be produced by mineral dehydration reactions within the downgoing slab [*Mottl et al.*, 2003; *Fryer et al.*, 2006]. The summit of South Chamorro Seamount is blanketed with recent (<0.45 Ma) pelagic biogenic sediments mixed with serpentinite muds containing large (up to several meters, based on ROV *Jason* 2 video camera survey) blocks of serpentinized peridotites and small metamorphic rock clasts, including blueschists [*Fryer et al.*, 2000; *Savov et al.*, 2005a; *Fryer et al.*, 2006] (Figures 4a–4d).

4. Petrographic and Textural Characteristics

[11] At ODP Hole 1200A, recovery was low, and we collected almost exclusively hard rocks of serpentinized peridotite clasts. This low recovery was caused by circulating drilling mud during rotary coring. At all other holes we used hydraulic piston coring or extended core barrel procedures, and the recovered materials were nearly 100% serpentinite mud. The hard rock clasts at Hole 1200A are heavily serpentinized and tectonized harzburgites and dunites: 98% of the recovered materials were harzburgites, and only 2% were dunites. The maximum recovered thickness of a single ultramafic clast was 110 cm.

[12] The petrography of the serpentinized ultramafic rocks was determined through microscopic observation and description of 57 thin sections. Petrographic details such as mineral abundances, textural types and thin section photomicrographs can be found in the ODP Leg 195 initial report [*Salisbury et al.*, 2002]. Inferences as to protoliths are based on observations of relict minerals and textures or on bulk rock composition when serpentinization is advanced. The composition and origin of the serpentinite muds and the metamorphic schists are discussed in separate publications [*Lockwood*, 1972; *Fryer*, 2002; *Savov et al.*, 2005a; *Fryer et al.*, 2006].

[13] The serpentinized harzburgites range in color from bluish gray to dark bluish gray (Figures 4a–4c). Grain size is highly variable, from fine- to coarse-grained (0.01–5 mm). The primary mineralogy includes olivine, orthopyroxene, clinopyroxene, and chromian spinel (see Figures 5a–5d). The samples display mesh and hourglass textures when the serpentinization involves olivine, and bastitic textures when orthopyroxene is serpentinized (Figures 4c and 5c). Relict olivine is generally anhedral and fine-grained (average diameter equals 0.05 mm), with kink banding evident in larger grains (Figure 5b). Orthopyroxene (OPX) crystallizes as equant, subhedral grains (average length ~1 mm) that often show undulose extinction (Figure 5a). Clinopyroxene (Cpx) occurs as small grains when present. Dark red, translucent spinels appear as small euhedral to anhedral grains (Figure 5a). The degree of serpentinization in the harzburgite samples ranges from 40 to 100% (average ~75%). In most cases, protolith mineralogy is impossible to infer directly because of pervasive serpentinization. Shipboard X-ray diffraction (XRD) data [*Salisbury et al.*, 2002], as well as electron microprobe [*D'Antonio and Kristensen*, 2004], ion probe [*Zack et al.*, 2004] and time-of-flight Secondary Ion Mass Spectrometry imaging (TOF-SIMS) [*Savov et al.*, 2006], all indicate that lizardite is the most common serpentine group mineral, usually accompanied by chrysotile and brucite. New time-of-flight SIMS measurements (1 μm resolution per pixel, 500 × 500 μm image size) of Leg 195 serpentinites (including micron size chri-

Figure 2. (a) Plane view of the South Chamorro Seamount. Note the traces of possible fault escarpments (marked with arrows). (b) Three-dimensional view of the South Chamorro Seamount. Note the presence of possible recent mudflow(s) on the flanks of the seamount (marked with arrows).

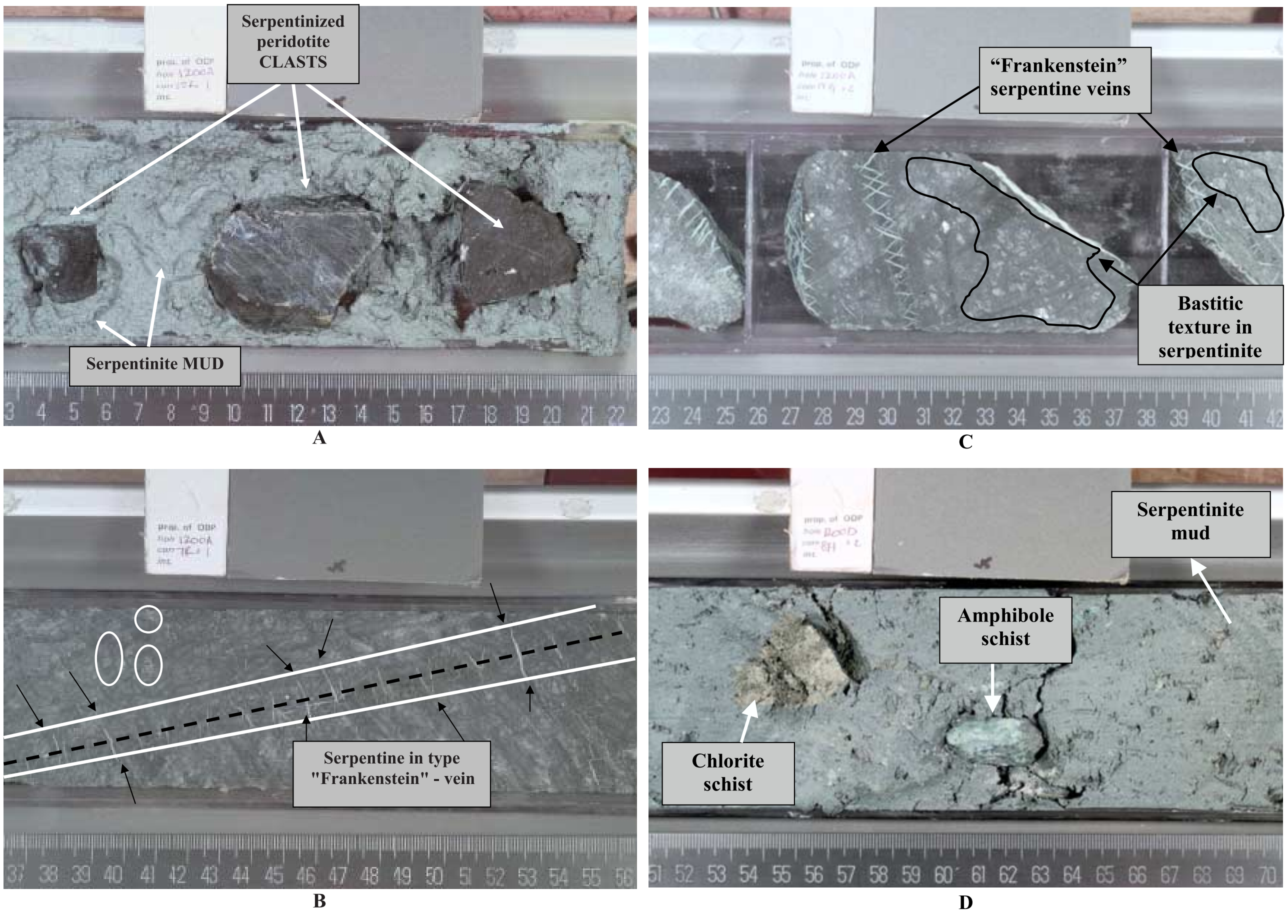

Figure 4. (a) Section of core 15R-1 from ODP Hole 1200A. Three serpentinized peridotite clasts are completely surrounded by serpentinite mud matrix. Note the scale at the bottom (in cm). (b) Section of core 7R-1 from ODP Hole 1200A. A large serpentinized peridotite clast is diagonally crosscut by "Frankenstein"-type serpentine vein. The central part of the vein is marked with dashed line and with solid line are marked vein boundaries. Note that the thickness of the reworked zone of preexisting serpentinite reaches 2 cm. Circles mark very large former orthopyroxene grains creating bastitic textures. (c) Section of core 17G-2 from ODP Hole 1200A showing several large serpentinized peridotite clasts. All clasts are crosscut by "Frankenstein"-type second generation serpentine veins. (d) Section of core 8H-2 from ODP Hole 1200E. Several types of metamorphic schists are incorporated in serpentinite mud matrix. The size of the clasts shown is up to 3 cm in diameter, but generally the metamorphic rock fragments are very small.

sotile veins) confirm that B and Li reside in the structure of the serpentine minerals [*Savov et al.*, 2006].

[14] Clinopyroxene and spinel are the minerals least affected by serpentinization, though sometimes chromite is partially altered to magnetite. Magnetite also appears in veins and in dust-like aggregates as a by-product of serpentinization, and rarely as small euhedral crystals. Amphibole (tremolite, actinolite, and Mg hornblende) and chlorite may be found as pyroxene replacement phases [*Zack et al.*, 2004] but are usually $\ll$1% of the rock volume.

[15] Serpentinized dunites range from very dark gray to dark bluish gray, and are generally fine grained (0.01–1 mm). The relict mineralogy consists of olivine, orthopyroxene, and Cr spinel. The recovered dunites are all extensively serpentinized (60–100%) and contain mesh textures with "hourglass" extinction where olivine has been replaced by serpentine and brucite. The dunites are crosscut by multiple generations of veins, composed mostly of serpentine and chlorite that sometimes includes significant concentrations of magnetite.

5. Analytical Methods

5.1. Major and Lithophile Trace Elements

[16] A suite of 27 representative serpentinized peridotites were analyzed for major and some trace elements onboard R/V *JOIDES Resolution* using JY 2000 inductively coupled plasma–atomic emission spectrometer (ICP-AES). Another suite of 70 serpentinized peridotites were analyzed for major and some trace elements via direct coupled plasma–atomic emission spectrometer (DCP-AES) at the University of South Florida, Tampa, Florida. Sample digestions for major and some trace elements (Cr, Ni, V, Zn, Cu, Mn) were performed on $LiBO_2$ fluxed fusions following the procedures described by *Savov et al.* [2005a]. Concentrations of the elements of interest are accurate within $\sim$10%, based on

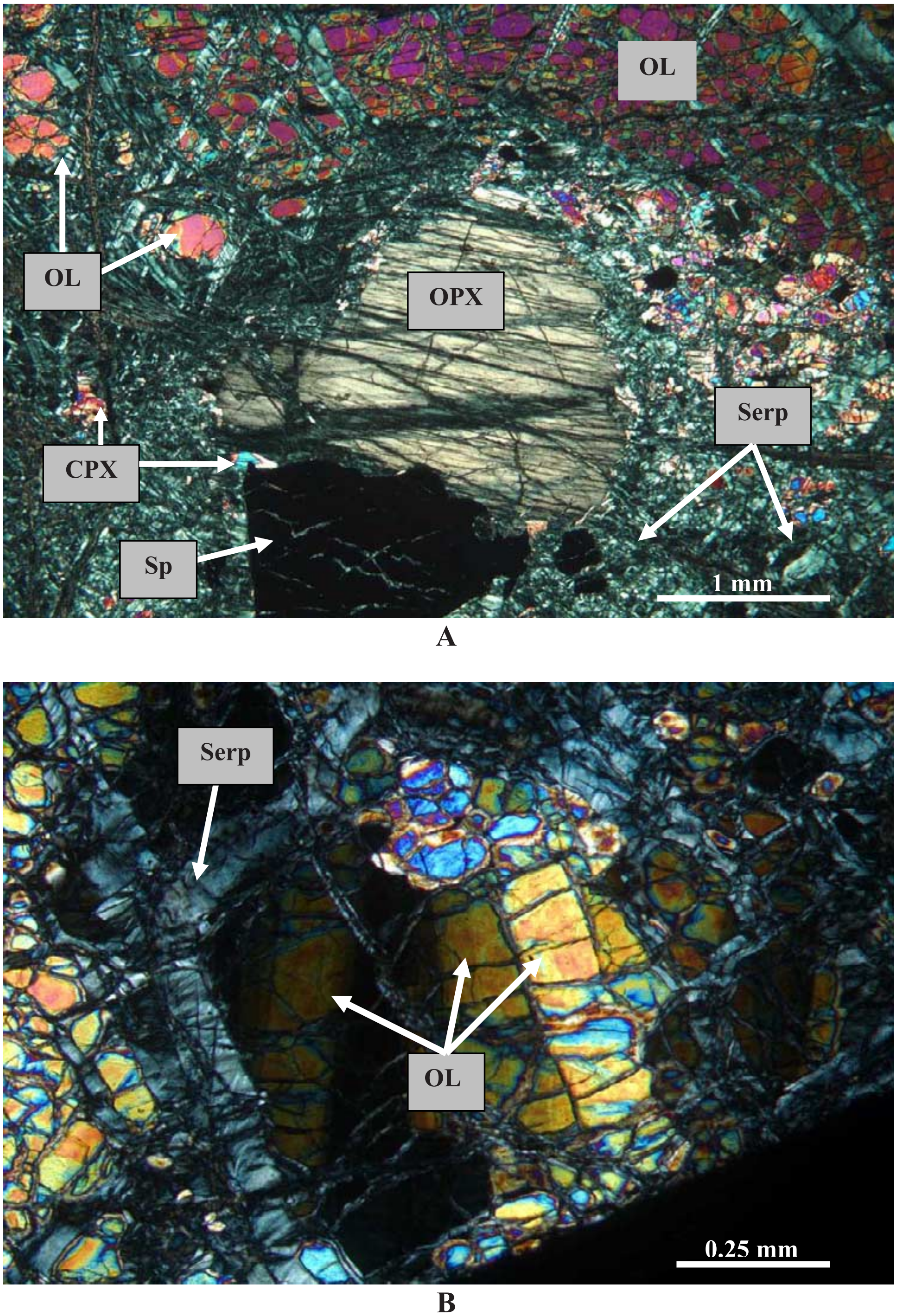

Figure 5. (a) Photomicrograph of sample 1200A-12R-1- (25-27)-3 showing relatively unaltered peridotite with relics of unaltered olivine (OL), orthopyroxene (OPX) and spinel (Sp). Serpentine, Serp. Note that the rims of the OPX grain are darker than the center. (b) Photomicrograph of olivine (OL) showing wavy extinction due to kink banding. A rim of serpentine (Serp) surrounds the olivine revealing that the serpentinization of this grain is incomplete. Same sample as in Figure 5a. (c) Mesh and hourglass textures in serpentinized peridotite sample 1200A-14R-1- (22–25)-10. Olivine, OL; and serpentine; Serp. (d) Photomicrograph of sample 1200A-7R-2- (27–29)-1A, showing several generations of serpentine (marked I and II) involved in the creation of Frankenstein-type veining patterns as shown in serpentinized peridotites in Figures 4b and 4c.

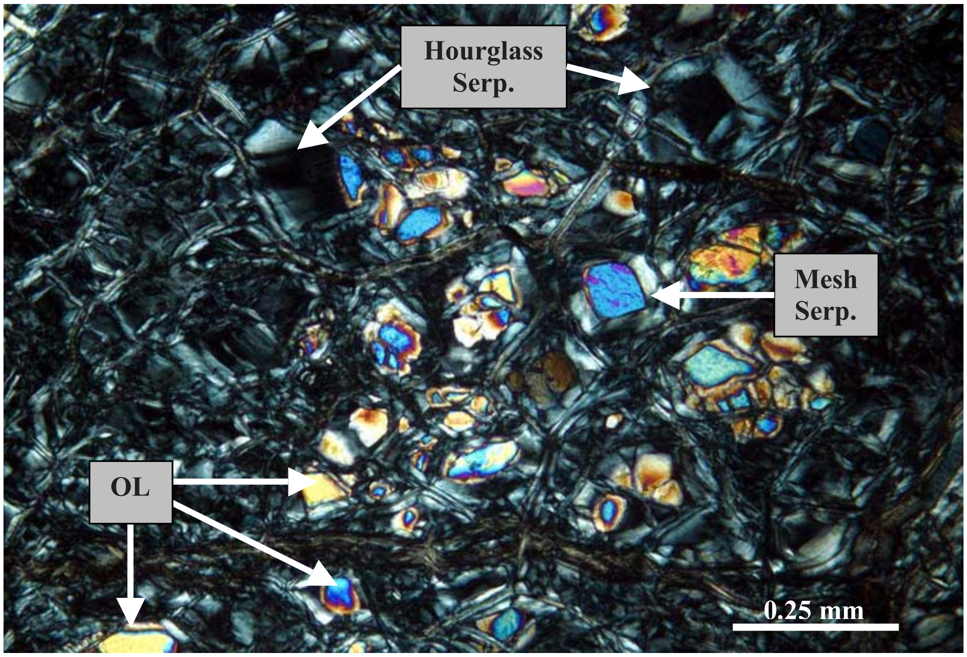

C

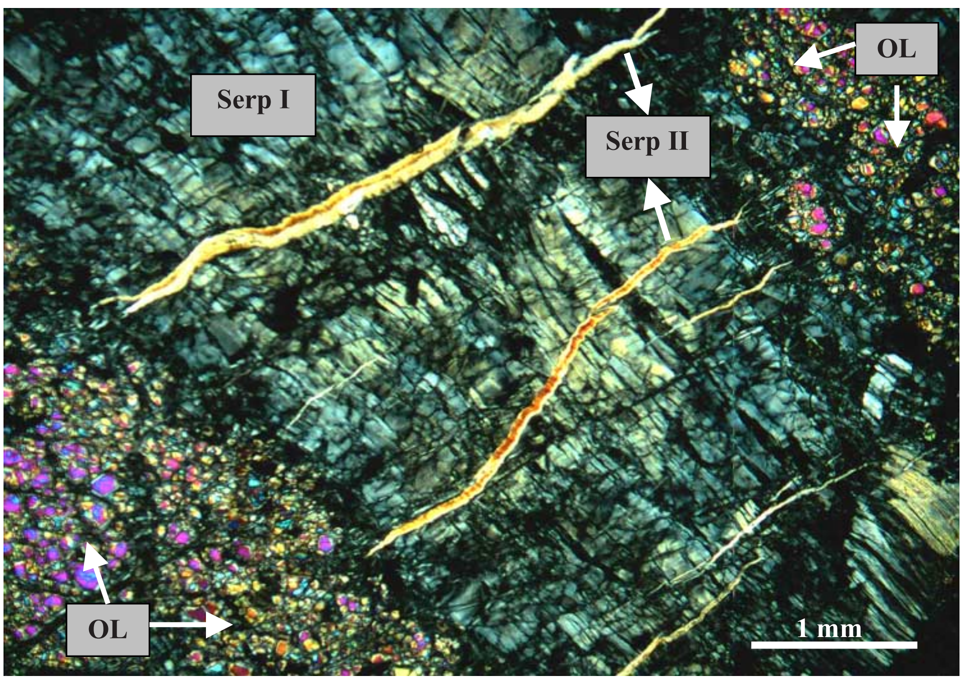

D

Figure 5. (continued)

monitoring by replicates of certified U.S. Geological Survey and Geological Survey of Japan standards: DTS-1, UBN-1, JP-1, BIR-1, and W-2. Analytical precision based on University of South Florida (USF) samples BC-1 (troctolite) and RR-1 (diabase) is reported in auxiliary material Table S1.[1]

[1]Auxiliary materials are available at ftp://ftp.agu.org/apend/jb/2006jb004749.

5.2. Low-Level Trace Elements

[17] A subset of the serpentinites was analyzed for rare earth elements (REE); Y, Sr, Li, Rb, Cs, Pb, As, Sb, U, Th, Nb, Ta, Hf, Zr, Sc, V, Ga, Cu, and Zn using the VG Elemental PlasmaQuad II ICP-MS facility at the Department of Earth Sciences of Boston University, Boston, Massachusetts. Samples were digested in 3:1 HNO_3: HF mixtures, following procedures described by *Kelley et al.* [2003]. Gravimetric calibration standards were matrix-

matched to sample solutions by adding ~150 ppm Mg from a 1000 ppm Mg standard solution (SPEX, Metuchen, New Jersey). The BaO interference on the Eu is typically <0.2%, so it is only important if Ba is orders of magnitude higher than Eu, which it is not the case in our samples. We tracked the BaO issue by running two Eu isotopes (^{151}Eu and ^{153}Eu). The interference should be larger on ^{153}Eu (because ^{137}Ba^{16}O is more abundant than ^{135}Ba^{16}O), which was not the case. The accuracy of our ICP-MS elemental data are considered in auxiliary material Table S2. One of the challenges of measuring refractory peridotites is their very low abundances of many trace elements critical to studies of subduction zone processes (REE, HFSE, U, Th, Pb, As, etc.). An important complicating factor is the lack of precise and accurate data for ultramafic standard reference materials: For many of the above elements, reported values vary by >100%. To try and address this problem, a range of standard reference materials (JB-3, BIR-1, PCC-1, JP-1, and DTS-1) were run as unknowns with each set of samples analyzed, such that each reference material was measured 4–6 times. On the basis of replicate analyses of the reference samples, reproducibility was about 5% for the higher concentration elements, and $\geq \pm10\%$ for the lowest concentration elements such as Zr, Hf, Nb, REE, As and Sb. The accuracy of our results is within 5–10% of reported values for all elements in our basaltic reference materials, but varies widely on an element-by-element basis in the ultramafic reference samples. Given the challenges in standardization for ultramafic rocks, what we have sought to do is produce an internally coherent geochemical data set for the serpentinites.

5.3. Arsenic Analysis

[18] Serpentinized peridotites from ODP sites 895D, 897D and 920D and 1200A were digested in warm aqua regia and analyzed for As by atomic fluorescence spectrophotometry (AFS) at the USF Geology Department. Arsenic concentrations measured by AFS are lower by ~30% relative to ICP-MS measurements, but the AFS determinations are in better agreement with reported ultramafic rock standard values. We also analyzed As in 42 pore fluid samples from ODP Site 1200. Sample splits from several of these pore fluid samples were also measured via AFS at University of Hawaii (School of Ocean and Earth Science and Technology) (M. Mottl, unpublished data, April 2007) and reproducibility was within ~5% of less from the values measured at USF (see auxiliary material Table S3).

5.4. Lithium and Boron Analyses

[19] Lithium abundances were measured via DCP-AES, following HF: $HClO_4$ (4:1) sample digestion using the procedures of *Ryan and Langmuir* [1987]. All Li determinations were performed via standard additions methods, using a gravimetric Li standard made from 99.999% pure Li_2CO_3. Reproducibility obtained for Li determinations was ±5% down to the 1 ppm Li level. Boron abundances were measured at USF on DCP-AES following a Na_2CO_3 fluxed fusion method, modified from that of *Ryan and Langmuir* [1993] in that as a final step all solutions were neutralized with ultrapure HNO_3, and no column preconcentration procedures were used. The majority of the measured serpentinized peridotite clasts have B > 10 ppm, and thus the DCP-AES reproducibility for all samples is better than 5%.

5.5. Sr Isotopes

[20] Sr isotope measurements were carried out at Istituto Nazionale di Geofisica e Vulcanologia, Osservatorio Vesuviano, Naples, Italy. Strontium was extracted via conventional ion exchange chromatographic techniques in an isotope clean laboratory facility. The samples were not leached so as to preserve their original Sr isotopic compositions. Measurements were made by thermal ionization mass spectrometry (TIMS) techniques on a ThermoFinnigan Triton TI multicollector mass spectrometer running in static mode. The normalization value for fractionation of Sr isotopes was $^{86}Sr/^{88}Sr = 0.1194$. External precision (2 sigma) for Sr isotope ratios from successive replicate measurements of the NIST SRM-987 International Reference Standard was better than 10 ppm (average $^{87}Sr/^{86}Sr = 0.710249$; n = 29; standard deviation equals 6.6×10^{-6}). The total blank for Sr was negligible for the measured samples during the period of measurements.

6. Whole Rock Chemistry

6.1. Major Element Variations

[21] New major, minor and trace element data on 70 serpentinized peridotites, as well as shipboard analysis for 27 serpentinized peridotites are reported in Tables 1a, 1b, 2a, and 2b. All of these samples are extensively serpentinized and hydrated [50 to 100%], with average loss on ignition (LOI) values ranging between 14 and 18 wt %. Shipboard LOI determinations were somewhat lower than LOI determinations made at USF (~14 wt % on average, as compared to ~17 wt %) but the USF samples were intentionally selected to represent the most highly modified peridotites. We present our results on the volatile-free basis to facilitate comparisons.

[22] While during serpentinization and low-temperature peridotite alteration some loss of MgO is documented [see *Kelemen et al.*, 2004], the magnitude of this loss is small relative to variations in other elements, such that comparisons to MgO still provide useful information about protolith compositions and elemental mobility. CaO and Al_2O_3 show distinct inverse correlations with MgO (Figures 6a–6b), consistent with the fact that both elements are concentrated in minor phases (Cpx, spinel) that vary inversely in abundance with primary olivine and orthopyroxene. The CaO and Al_2O_3 data reveals some scatter, possibly caused by the sensitivity of CaO and Al_2O_3 to previous melt extraction events and/or the presence of aluminous phases. The observed arrays for the South Chamorro Seamount samples are similar to those seen for serpentinized peridotites from Conical Seamount [*Parkinson and Pearce*, 1998; *Savov et al.*, 2005b].

[23] As a whole, the reported data set reveals that the recovered serpentinized peridotites are all MgO-rich with high Ni and Cr contents (average equals 3920 ppm and 2910 ppm for Ni and Cr, respectively). Mg numbers (Mg #) range from 91 to 93, and the average Si/Mg ratio is 0.92. The average Al_2O_3 (0.36 wt %), CaO (0.47 wt %) and TiO_2 (0.005 wt %) contents are very low, consistent with low

Table 1a. Shipboard ICP-AES Major and Trace Element Data for South Chamorro Seamount Serpentinized Peridotites for Site 1200[a]

	Depth, mbsf													
	19.01	41.71	51.96	52.38	52.85	80.03	80.83	80.90	89.60	89.68	90.03	99.03	108.95	109.33
Hole	A	A	A	A	A	A	A	A	A	A	A	A	A	A
Core-section	3R-1	6R-1	7R-2	7R-2	7R-2	10R- 1	10R-1	10R-1	11R-1	11R-1	11R-1	12R-1	13R-1	13R-1
Interval	81–84	31–33	27–29	69–71	116–118	13–15	93–95	100–102	20–24	28–30	63–65	3–5	25–27	63–65
Piece	2	2	1A	1C	2	3	11	12	6	7	11	1	6	7
SiO_2, wt %	43.76	41.12	44.05	43.14	44.41	42.90	43.12	44.26	43.98	44.08	43.99	44.42	41.34	43.81
TiO_2	0.01	0.01	0.01	0.01	0.01	0.01	0.02	0.02	0.02	0.02	0.01	0.01	0.01	0.01
Al_2O_3	0.56	0.62	0.72	0.73	0.70	0.72	0.95	0.82	0.84	0.68	0.71	0.64	0.62	0.39
Fe_2O_3T	8.33	8.71	8.26	8.33	8.13	8.32	8.28	8.45	8.62	8.66	8.84	7.95	9.80	8.33
MnO	0.11	0.11	0.12	0.12	0.12	0.13	0.11	0.12	0.13	0.11	0.12	0.12	0.15	0.12
MgO	46.50	48.69	47.15	46.68	46.26	47.56	45.30	46.02	46.57	46.64	47.41	46.27	48.37	46.87
CaO	0.59	0.63	0.75	0.91	0.86	0.49	1.82	0.95	0.53	0.77	0.73	0.71	0.36	0.37
Na_2O	0.09	0.07	0.08	0.06	0.05	0.11	0.10	0.10	0.15	0.04	0.08	0.07	0.08	0.08
K_2O	0.04	0.03	0.02	0.03	0.02	0.02	0.03	0.03	0.01	0.02	0.03	0.03	0.02	0.02
P_2O_5	0.03	0.01	0.04	0.01	0.06	0.06	0.01	0.06	0.04	0.06	0.01	0.01	0.01	0.00
Total	100.0	100.0	100.9	100.0	100.6	100.2	99.7	100.8	100.2	101.0	101.9	100.2	100.8	100.0
LOI	14.5	14.6	12.9	11.3	11.6	16.7	14.5	15.6	11.7	12.5	13.5	12.4	18.2	13.7
V	29	25	18	18	19	31	43	39	42	28	31	19	30	20
Cr	2487	3685	2897	2973	2660	2340	3170	2251	3193	2739	2977	2806	2548	2360
Ni	2342	2558	2524	2384	2464	2721	2403	2541	3339	2588	2503	2432	3706	2879
Sr	19.5	26.8	15.8	16.1	13.3	31.6	34.8	41.7	24.9	9.8	24.5	7.3	18.9	16.5
Ba	4.8	2.8	3.3	3.4	7.5	8.2	5.6	12.8	6.8	7.6	3.7	10.7	2.2	6.6
B		13.5				22.2						23.4	19.5	
Li		2.3	1.5	1.6	2.5			2.8	1.2	2.1	5.6	8.5	2.6	8.4

Table 1a. (continued)

	Depth, mbsf														
	109.60	118.52	118.59	137.81	138.72	138.93	139.10	139.24	139.43	Unknown	0.76	32.22	0.66	2.40	3.89	7.80
Hole	A	A	A	A	A	A	A	A	A	A	B	B	D	D	D	D
Core-section	13R-1	14R-1	14R-1	16R-1	16R-1	16R-1	16R-2	16R-2	16R- 2	17G - 2	1W- 1	2W- 2	1H- 1	1H- 2	1H- 3	2H- 1
Interval	90–92	22–24	29–31	21–23	112–114	133–135	15–17	29–31	48–50	29–31	76–78	2–6	66–70	94–98	89–93	90–92
Piece	8B	6A	7	5	11B	12	1	2	4	2	5B	1				
SiO_2, wt %	43.26	42.81	45.08	43.70	42.86	43.85	44.63	43.22	44.21	44.23	41.67	42.95	47.02	45.68	42.27	44.24
TiO_2	0.01	0.01	0.02	0.01	0.01	0.01	0.01	0.01	0.01	0.01	0.01	0.01	0.01	0.01	0.01	0.01
Al_2O_3	0.49	0.62	0.99	0.36	0.45	0.37	0.72	0.67	0.38	0.70	0.41	0.37	0.94	0.23	0.22	0.48
Fe_2O_3T	8.62	8.70	8.17	8.62	7.99	7.76	7.78	8.31	8.57	8.15	8.56	7.60	8.24	8.02	8.09	8.24
MnO	0.11	0.12	0.13	0.12	0.12	0.12	0.12	0.12	0.12	0.12	0.13	0.12	0.11	0.11	0.13	0.13
MgO	47.79	46.81	44.52	46.53	46.02	47.30	47.12	46.58	47.38	47.20	48.87	46.33	43.52	45.86	49.16	46.49
CaO	0.69	0.82	1.01	0.55	0.66	0.69	0.93	0.98	0.46	0.78	0.24	0.67	0.07	0.06	0.08	0.28
Na_2O	0.07	0.06	0.07	0.11	0.07	0.07	0.07	0.07	0.27	0.10	0.09	0.07	0.07	0.03	0.03	0.11
K_2O	0.03	0.03	0.02	0.01	0.02	0.02	0.03	0.03	0.03	0.03	0.01	0.02	0.01	0.00		0.02
P_2O_5	0.01	0.01	0.00	0.00	0.05	0.01	0.06	0.01	0.01	0.05	0.04	0.04	0.00	0.00	0.00	0.00
Total	101.1	100.0	100.0	100.0	98.2	101.2	101.4	100.0	101.4	101.3	100.0	100.0	100.0	100.0	100.0	100.0
LOI	14.5	14.0	11.9	16.8	15.6	15.9	12.0	13.1	16.0	14.9	16.0	11.4	13.8	13.0	19.3	15.3
V	23	19	39	18	26	23	19	19	28	32	27	17	42	14	13	23
Cr	2564	2552	3449	1610	3810	2201	2427	2492	2661	3175	2178	2551	2647	2505	4508	3202
Ni	2437	2580	3821	3110	2483	2761	2412	2524	2829	2673	2983	2879	4505	2638	3162	2730
Sr	23.7	18.2	12.2	40.8	21.6	18.0	17.1	17.0	24.2	29.4	12.7	7.9	6.4	1.6	2.2	13.9
Ba	3.0	4.7	7.3	6.1	9.2	5.3	13.1	9.8	7.2	8.7	2.4	2.7	5.3	4.4	4.1	6.5
B						32.0			19.7							
Li	2.6	2.5	3.6	0.7	1.2	0.6	1.9		0.5				8.6	0.3	0.5	2.8

[a]Oxides and LOI in weight percent, all other elements in ppm. All of the elements are presented on an anhydrous basis. See text for analytical precision. B and Li abundances were measured on DCP-AES at USF using shipboard powders.

Table 1b. Average Shipboard Samples From Depth >50 mbsf

Element	Value
SiO_2, wt %	43.61
TiO_2	0.01
Al_2O_3	0.65
Fe_2O_3T	8.41
MnO	0.12
MgO	46.86
CaO	0.76
Na_2O	0.09
K_2O	0.02
P_2O_5	0.03
Total	100.5
LOI	14.1
V, ppm	27
Cr	2763
Ni	2725
Sr	21.9
Ba	6.8
B	21.7
Li	2.8

clinopyroxene abundances, and the overall depleted character of the serpentinite protoliths.

6.2. Trace Element Variations

[24] Trace element data for the serpentinized peridotites from ODP Site 1200 holes A, D, E, and F are compiled in Tables 3a and 3b and are presented in Figures 7–10 in comparison to the well studied fore-arc-serpentinized peridotites of Conical Seamount drilled during ODP Leg 125 [*Savov et al.*, 2005b]. The majority of the analyzed samples are from the Hole 1200A, but the other sites reveal the same abundance patterns. Unless specifically noted, we will review their geochemistry as a group, rather than hole by hole.

6.2.1. B, Cs, As, Sb, Rb, Pb, Li, K, Sr, Ba, U, and Th

[25] In Figure 7 we have plotted the variations of the FME [see *Leeman*, 1996; *Noll et al.*, 1996] as well as the lithophile elements Li, K, Sr, Ba, U and Th versus core depth for each drill site. We observe no correlation between the degree of serpentinization (expressed as LOI wt %) and the abundances of FME and Th.

[26] Boron, As, Cs, and Rb all show dramatic enrichments in the Hole 1200 samples relative to mantle values (Figures 7a–7g, see also Figures 8a–8b) much as is observed in the Conical Seamount serpentinized peridotites, although abundances and patterns of downhole variation differ. At South Chamorro Seamount B is moderately elevated in the first 20 m in the core and varies around a mean of ~25 ppm B at depth, while Conical Seamount serpentinized peridotites reach higher B abundances at shallow core depths, and lower B abundances at greater depths. Mean Cs abundances are lower in the South Chamorro Seamount suite than in the Conical Seamount suite (0.15 versus 0.27 ppm) but both are dramatically higher than depleted upper mantle. Arsenic abundances are modestly lower in South Chamorro Seamount than at Conical Seamount (0.33 ppm versus 0.48 ppm), and much like B, are associated with elevated pore fluid concentrations [*Mottl*, 1992; *Mottl et al.*, 2003] (Figure 7c; see auxiliary material Table S3).

[27] Lithium, Sb, and Sr all indicate modest overall enrichments in the South Chamorro peridotites relative to depleted mantle values (Figures 7b–7h). The abundance levels and variation patterns are generally similar to what is observed at Conical Seamount, though Li is lower in abundance overall (~2.5 ppm versus ~4.6 ppm), and Rb is higher (0.74 ppm versus 0.45 ppm).

[28] Barium and Pb abundances in serpentinized peridotites from South Chamorro and Conical Seamount are similar and resemble the values reported for depleted mantle by *Salters and Stracke* [2004] (Figures 7e, 7i, and 8). Uranium and Th abundances are very low in clasts from both sites, and are on average lower than reported depleted mantle values (Figure 8).

Table 2a. DCP-AES Major and Trace Element Data for South Chamorro Seamount Serpentinized Peridotites for Site 1200[a]

	Depth, mbsf																
	18.23	18.3	19.01	41.75	41.97	42.99	43.05	51.14	51.35	51.72	52.09	52.38	52.83	52.99	70.46	70.54	70.81
Hole	A	A	A	A	A	A	A	A	A	A	A	A	A	A	A	A	A
Core-section	3R-1	3R-1	3R-1	6R-1	6R-1	6R-2	6R-2	7R-1	7R-1	7R-2	7R-2	7R-2	7R-2	7R-2	9R-1	9R-1	9R-1
Interval	3–7	10–12	81–84	35–37	57–59	33–35	39–41	4–6	25–27	3–5	40–43	69–71	114–117	130–132	6–8	14–16	41–43
Piece	1A	1A	2	2	8	1B	1B	2	2A	1A	1B	1C	2	1B	2	4B	6
SiO_2, wt %	41.16	42.97	41.92	42.05	41.18	38.85	41.75	42.27	41.55	42.89	42.25	41.73	42.61	41.42	41.08	35.60	38.69
TiO_2	0.000	0.020	0.004	0.008	0.016	0.009	0.010	0.003	0.000	0.003	0.005	0.000	0.004	0.011	0.010	0.003	0.004
Al_2O_3	0.47	0.49	0.46	0.54	1.14	0.42	0.53	0.48	0.56	0.67	0.59	0.68	0.70	0.68	0.73	0.12	0.10
Fe_2O_3T	8.70	8.28	8.43	8.68	8.52	9.21	8.99	8.56	8.27	8.22	8.50	8.03	8.51	8.19	8.83	9.83	8.70
MnO	0.12	0.12	0.12	0.12	0.12	0.12	0.13	0.12	0.12	0.12	0.12	0.11	0.12	0.12	0.13	0.14	0.12
MgO	47.43	47.89	46.60	46.85	47.44	49.57	48.66	47.91	47.09	47.06	48.71	47.18	47.22	46.45	47.07	53.10	52.38
CaO	0.74	0.25	0.34	0.22	0.57	0.35	0.37	0.37	0.64	0.57	0.38	0.58	0.70	0.70	0.31	0.11	0.11
Na_2O	0.07	0.08	0.08	0.16	0.10	0.06	0.14	0.25	0.06	0.10	0.10	0.05	0.06	0.05	0.25	0.13	0.13
K_2O	0.03	0.04	0.04	0.03	0.05	0.02	0.04	0.05	0.05	0.05	0.02	0.05	0.05	0.05	0.03	0.04	0.04
Total	98.72	100.13	97.99	98.67	99.16	98.61	100.64	100.02	98.35	99.64	100.67	98.41	99.96	97.65	98.44	99.09	100.28
LOI	15.9	15.1	15.2	18.7	14.6	15.6	17.0	14.2	12.9	14.3	16.1	11.7	13.2	14.3	20.2	18.0	19.3
V		44	56	57	43	33	51	37	40		23		39			34	39
Cr	3227	2879	2819	3094	4868	5665	2688	2254	1956	2339	2540	3809	3360	2840	4489	3905	2879
Ni		3328	1304	4309	5487	5011	3893	4834	4913	4394	3272		3814			6096	5408
Cu		10	14	25	8	14	15	8	11	1	8		13			11	10
Zn		53	61	63	77	59	59	64	65	53	52		52			66	59
B			33.0					18.9							4.1		
Li			8.9					2.3	1.8	1.8					1.2		

Table 2a. (continued)

	Depth, mbsf																
	80.1	80.25	80.85	89.56	89.68	89.8	89.95	99.03	108.76	108.82	108.95	109.33	109.91	109.98	110.07	118.39	118.59
Hole	A	A	A	A	A	A	A	A	A	A	A	A	A	A	A	A	A
Core-section	10R-1	10R-1	10R-1	11R-1	11R-1	11R-1	11R-1	12R-1	13R-1	13R-1	13R-1	13R-1	13R-1	13R-2	13R-2	14R-1	14R-1
Interval	20–23	35–37	95–97	16–18	28–30	40–42	45–47	3–5	6–8	12–16	25–27	63–65	121–124	3–5	12–15	9–11	29–31
Piece	5	6	11	6	7	8	8	1	2	8	6A	7	11	1A	2	8	7
SiO_2, wt %	40.48	41.72	44.36	40.33	41.77	41.52	42.68	38.53	40.94	38.01	39.33	42.40	41.90	41.41	40.61	34.67	42.06
TiO_2	0.010	0.005	0.000	0.000	0.010	0.003	0.010	0.004	0.004	0.010	0.007	0.003	0.005	0.000	0.005	0.006	0.010
Al_2O_3	0.65	0.51	1.01	0.01	0.64	0.36	0.47	0.67	0.56	0.27	0.49	0.78	0.59	0.36	0.69	0.50	0.94
Fe_2O_3T	8.32	7.93	9.07	8.10	8.32	8.48	8.09	9.48	9.19	8.03	9.60	8.55	8.25	8.52	9.60	10.82	8.23
MnO	0.12	0.11	0.13	0.09	0.12	0.12	0.12	0.16	0.14	0.11	0.15	0.13	0.12	0.12	0.15	0.17	0.11
MgO	49.79	47.40	46.22	49.77	46.48	49.87	46.73	48.88	48.46	52.97	48.10	48.32	47.06	47.30	50.00	51.36	45.00
CaO	0.34	0.51	0.58	0.27	0.71	0.34	0.31	0.26	0.36	0.20	0.21	0.46	0.53	0.38	0.35	0.19	0.55
Na_2O	0.15	0.06	0.11	0.26	0.07	0.11	0.14	0.16	0.15	0.11	0.16	0.13	0.07	0.19	0.14	0.15	0.08
K_2O	0.04	0.04	0.05	0.05	0.03	0.02	0.04	0.04	0.05	0.02	0.04	0.03	0.06	0.06	0.03	0.05	0.02
Total	99.89	98.29	101.53	98.87	98.13	100.83	98.57	98.19	99.85	99.72	98.08	100.78	98.55	98.33	101.61	98.00	97.01
LOI	18.4	14.0	15.9	23.4	13.0	18.0	16.4	17.5	13.8	16.8	19.0	15.0	13.3	8.8	17.7	19.0	14.0
V	43	40	84	27		34	59	50	59	42	45	35	22	30	47	43	
Cr	2982	2599	2341	1658	2750	3728	2691	3060	3444	2288	2671	2268	2702	2681	3633	2881	2903
Ni	4647	5290	4650	7087		4935	4028	1485	5303	6390	6253	3383	4992	6121	6062	5211	
Cu	13	9	12	4		8	17	14	12	13	12	8	6	8	9	10	
Zn	73	58	59	70		63	80	54	64	73	59	55	68	66	66	82	
B			10.7			6.8									10.2		
Li			2.3			3.4									2.5		

Table 2a. (continued)

	Depth, mbsf																
	128.01	138.88	139.11	139.43	>139.43	>139.43	>139.43	0.56	7.73	9.47	16.05	18.03	18.44	19.86	25.11	54.53	0.78
Hole	A	A	A	A	A	A	A	E	E	E	E	E	E	E	E	E	F
Core-section	15R-1	16R-1	16R-2	16R-2	17G-1	17G-2	17G-2	1H-1	2H-2	2H-3	4H-3	5H-1	5H-1	5H-2	6H-3	10H-2	1H-1
Interval	11–13	128–130	16–18	48–50	80–82	26–28	76–79	56–58	13–15	37–39	105–110	43–45	87–89	81–83	97–99	63–65	78–80
Piece		12	1	4	5		8										
SiO_2, wt %	40.26	40.95	41.74	42.57	39.01	41.96	41.55	37.66	41.55	42.70	42.98	40.39	41.25	41.76	41.77	42.22	41.18
TiO_2	0.004	0.000	0.003	0.000	0.009	0.009	0.006	0.009	0.010	0.000	0.000	0.002	0.002	0.010	0.010	0.010	0.001
Al_2O_3	0.32	0.53	0.68	0.36	0.42	0.58	0.46	0.65	0.96	1.36	1.07	0.48	0.57	0.32	0.33	0.37	0.47
Fe_2O_3T	9.03	8.60	8.52	8.14	8.92	8.69	7.94	8.12	8.42	8.23	8.37	8.71	8.57	8.56	8.85	8.37	8.33
MnO	0.12	0.12	0.13	0.11	0.12	0.13	0.12	0.12	0.11	0.13	0.12	0.12	0.12	0.13	0.11	0.12	0.10
MgO	48.04	47.92	46.94	47.37	47.71	47.98	47.84	42.16	45.71	44.88	45.38	48.71	48.34	46.68	48.20	46.93	46.06
CaO	0.72	0.56	0.87	0.33	0.34	0.55	0.28	9.22	0.07	0.41	0.60	0.18	0.56	0.16	0.26	0.46	0.07
Na_2O	0.26	0.08	0.10	0.17	0.07	0.11	0.11	0.16	0.23	0.17	0.11	0.10	0.08	0.04	0.00	0.16	0.24
K_2O	0.04	0.03	0.04	0.05	0.05	0.03	0.03	0.05	0.03	0.05	0.04	0.02	0.05	0.04	0.04	0.05	0.03
Total	98.82	98.81	99.04	99.09	96.62	100.06	98.32	98.15	97.09	97.94	98.69	98.71	99.54	97.71	97.05	98.68	97
LOI	19.3	15.7	13.8	19.3	15.4	16.2	16.5	22.6	16.2	15.6	12.5	15.5	24.9	20.8	19.8	19.8	18.7
V	66	58	38	44	43	48	217	75	70	113	61	52	47	62	52	65	
Cr	3129	6837	3221	1935	4506	3003	2733	3172	2648	3282	2064	3540	2539	2184	2323	2841	2845
Ni	5333	4756	3248	5320	4539	3285	3159	4700	5838	4814	5117	5652	6580	5807	5792	5636	
Cu	14	10	13	8	13	22	44	16	15	18	11	10	13	12	12	22	
Zn	83	73	58	77	72	53	160	69	66	65	65	70	68	73	80	71	
B	18.4		16.5			15.1	9.3		11.2			39.8		20.5	31.1	4.6	
Li	1.1		1.7			2.2	2.4									0.6	

Table 2a. (continued)

	Depth, mbsf					
	1.16	2.23	8.0	13.95	14.65	15.01
Hole	F	F	F	F	F	F
Core-section	1H-1	1H-2	2H-1	3H-1	3H-2	3H-2
Interval	116–118	73–76	30–32	105–107	25–27	61–63
Piece						
SiO_2, wt %	42.05	40.12	39.23	39.66	39.88	40.20
TiO_2	0.003	0.010	0.000	0.004	0.000	0.01
Al_2O_3	0.43	0.34	0.24	0.19	0.50	0.67
Fe_2O_3T	8.87	8.48	8.74	8.41	9.43	8.05
MnO	0.10	0.12	0.13	0.12	0.14	0.12
MgO	46.00	47.56	50.69	51.01	48.83	42.47
CaO	0.41	0.27	0.10	0.11	0.06	9.00
Na_2O	0.33	0.13	0.14	0.06	0.43	0.18
K_2O	0.06	0.05	0.17	0.05	0.08	0.06
Total	98.25	97.06	99.31	99.58	99.29	100.75
LOI	21.3	14.7	16.9	17.0	17.0	16.8
V	53	57			43	23
Cr	4034	2349	3107	3233	4610	2077
Ni	7733	5595			6391	5473
Cu	9	9			10	13
Zn	67	68			60	55
B		34.1	26.0		32.5	
Li						

[a]Oxides and LOI in weight percent, all other elements in ppm. All of the elements are presented on an anhydrous basis. See text for analytical precision.

6.2.2. Rare Earth Elements

[29] The Leg 195 serpentinized peridotites have very low REE abundances, much like those in the Leg 125 serpentinites [*Savov et al.*, 2005b]. Yb and Y, shown to correlate with MgO in samples from Conical Seamount [*Parkinson and Pearce*, 1998] do not vary systematically with MgO in the South Chamorro Seamount suite. The serpentinized peridotites display REE abundances depleted relative to chondritic values by 1–2 orders of magnitude for the HREE (i.e., Lu through Dy) and the LREE (La through Sm), and by up to 3 orders of magnitude for the middle REE (MREE: Sm through Dy) (Figures 9a and 9b). $[La/Sm]_N$ in our samples ranges from 1 to 38 and $[Dy/Yb]_N$ varies from 0.02 to 0.27, resulting in overall U-shaped rare earth patterns. The heavy REE patterns resemble those of supra-subduction zone peridotites, and are indicative of a high degree of fractional melt extraction [*Pearce et al.*, 2000; *Bodinier and Godard*, 2003]. Many of our samples show large positive Eu anomalies, caused by the differential mobility and enrichment of Eu^{2+}. Positive Eu anomalies are also observed in Conical Seamount serpentinized peridotites [*Parkinson and Pearce*, 1998; *Savov et al.*, 2005b]. Measured Eu in reference materials DTS-1, JP-1, and PCC-1 are in reasonable agreement with reported literature values, and there is also no correlation between LOI values and the Eu anomalies, suggesting that on chondrite-normalized REE plots the elevated Eu (in respect to the adjacent Sm and Gd) is neither a product of serpentinization, nor an analytical artifact.

6.2.3. High Field Strength Elements

[30] Niobium, Hf, Zr, and Ti in our South Chamorro Seamount serpentinized peridotites are low, much like the Conical Seamount samples, and are comparable to the very low values seen in depleted mantle peridotites [*Salters and Stracke*, 2004] (Figure 8). Neither the HSFE nor the heavy rare earths show any systematic variation with LOI, indicating these elements have little sensitivity to alteration and low-temperature metamorphism, as noted previously by *Woodhead et al.* [1993] and *King et al.* [2006]. Like other abyssal and ophiolitic basement peridotites [*Bodinier and Godard*, 2003], the South Chamorro samples show a broad correlation between Al_2O_3 and Yb (HREE) ($R^2 \sim 0.52$) (Figure 10), but no correlation between Al_2O_3 and Ce (LREE) ($R^2 \sim 0.05$) or Al_2O_3 and Zr ($R^2 \sim 0.002$) (both not shown). This observation supports the idea that the less incompatible high field strength elements (Zr, Hf) show systematics similar to those observed for REE with similar $D^{S/L}$ values.

6.2.4. Strontium Isotope Ratios

[31] The Leg 195 serpentinized peridotites have $^{87}Sr/^{86}Sr$ ratios that are much lower than seawater [mean $^{87}Sr/^{86}Sr \approx 0.7050$], but are elevated relative to the range of depleted

Table 2b. Average Onshore Samples From Depth >50 mbsf

Element	Value
SiO_2, wt %	40.97
TiO_2	0.005
Al_2O_3	0.55
Fe_2O_3T	8.62
MnO	0.12
MgO	47.82
CaO	0.69
Na_2O	0.13
K_2O	0.04
Total	98.91
LOI	16.6
V, ppm	52
Cr	3072
Ni	4931
Cu	12
Zn	67
B	19
Li	2.5

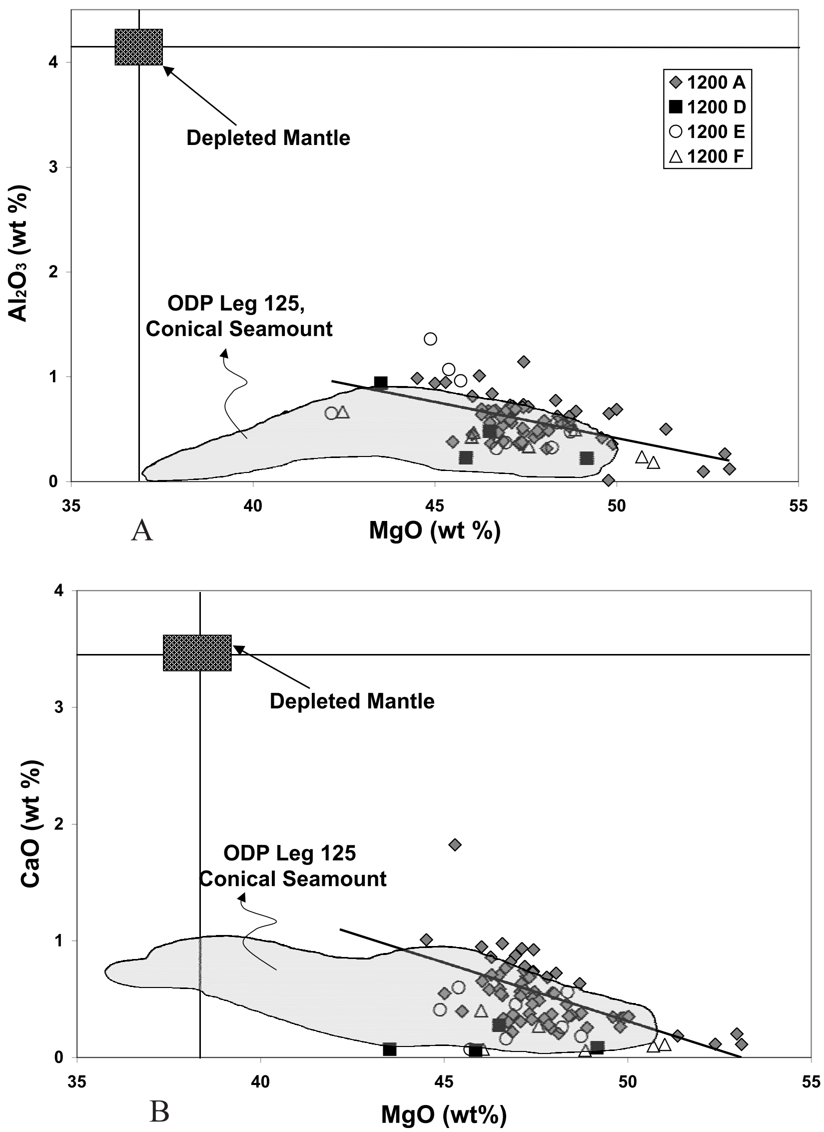

Figure 6. Co-variation diagram of MgO with (a) Al_2O_3 and (b) CaO in serpentinized peridotites from ODP Site 1200. Diamonds (Hole A); squares (Hole D); circles (Hole E), and triangles (Hole F). The depleted mantle values are from *Salters and Stracke* [2004] and *Walter* [2003]. The best fit line through the Leg 195 data is shown as solid line.

mantle rocks reported by *Salters and Stracke* [2004] and the Geochemical Earth Reference Model (GERM) database (http://earthref.org/GERM/index.html). The ratio $^{87}Sr/^{86}Sr$ shows no correlations with either LOI or 1/Sr. The sample with the highest $^{87}Sr/^{86}Sr$ is at the top of the depth profile ($^{87}Sr/^{86}Sr$ = 0.70551) (Figure 11, see Table 4).

7. Discussion

[32] The serpentinized ultramafic samples from the Mariana fore-arc drill sites represent a new variety of mantle wedge material. Our results indicate that though this type of mantle rock is generated at shallow depths and significant distances from the Mariana volcanic arc, it is probable that such rocks are involved in the genesis of arc magmas in the Marianas, and perhaps in other arcs, entailing some changes in current models for slab-mantle exchange processes.

7.1. Comparisons With Other Marine Serpentinite Occurrences

[33] While the South Chamorro and other Mariana fore-arc serpentinites are similar to a first order to serpentinites present in the Franciscan formation and other preserved fore-arc accretionary sequences [*Lockwood*, 1972; *Bebout*, 1995; *Bebout and Barton*, 2002; *Fryer et al.*, 2000; *King et al.*, 2003, 2006], so far only one intraoceanic fore-arc serpentinite locality is known outside the Mariana subduction system for which high-quality geochemical data are available: the South Sandwich fore-arc region, from which only dredged samples have been recovered [*Pearce et al.*, 2000]. The Conical Seamount, in the northern Mariana fore arc, ~1000 km north of South Chamorro, was drilled and analyzed in association with ODP Leg 125 [see *Fryer et al.*, 1992; *Parkinson et al.*, 1992; *Parkinson and Pearce*, 1998; *Benton et al.*, 2001, 2004; *Savov et al.*, 2005a, 2005b] and

Table 3a. ICP-MS Trace Element Data for South Chamorro Seamount Serpentinized Peridotites for Site 1200[a]

	Depth, mbsf																								
	19.01	41.75	43.23	45.35	51.14	51.72	70.46	80.03	80.85	89.8	90.09	99.03	108.95	110.07	128.01	138.93	139.11	139.43	>139.5	>139.5	18.03	19.86	54.53	28.6	14.65
Hole	A	A	A	A	A	A	A	A	A	A	A	A	A	A	A	A	A	A	A	A	E	E	E	E	F
Core-section	3R-1	6R-1	6R-2	6R-3	7R-1	7R-2	9R-1	10R- 1	10R-1	11R-1	11R-1	12R-1	13R-1	13R-2	15R-1	16R-1	16R-2	16R-2	17G-2	17G-2	5H-1	5H-2	10H-2	7H-2	3H-2
Interval	81–84	35–37	35–37	97–99	4–6	3–5	6–8	13–15	95–97	40–42	69–72	3–5	25–27	12–15	11–13	133–135	16–18	48–50	26–28	76–79	43–45	81–83	63–65	121–123	25–27
Li	9.3	2.6	2.6	0.6	5.4	1.8	1.1	2.3	2.4	4.1	7.3	7.7	3.0	2.8	1.0	0.7	1.6	0.5	2.1	2.5	1.5	0.4	0.5	3.6	5.2
Sc	5.8	5.4	4.4	4.6	6.6	8.0	9.2	6.2	9.0	5.2	6.9	8.3	7.2	7.3	6.9	6.7	7.6	7.5	6.6	5.2	4.4	6.3	5.5	7.6	7.1
TiO_2, wt %				0.002			0.003				0.005	0.001			0.003		0.004		0.006			0.001	0.004		
V							20.4				11.9	4.4			6.1		5.1		12.5			2.1	3.7		
Cr				1228			8300				2892	3194			2468		3240		2946			2041	1930		
Co				101			112				97	103			95		98		100			101	94		
Ni				2358			2617				2086	2439			2245		1991		2111			2384	2313		
Cu	8		8		4	1			3					2						2	2			4	5
Zn				51			42				26	40			64		29		28			40	42		
Ga	0.3		0.1	0.0	0.3	0.4	0.5		0.5		0.2	0.5		0.3	0.2		0.3		0.3	0.2	0.2	0.2	0.2	0.3	0.2
As	0.25	0.32	0.32	0.27	0.17	0.30	0.23	0.48	0.31	0.36	0.28	0.36	0.52	0.52	0.24	0.49	0.15	0.48	0.23	0.21	0.11	0.24	0.20	0.34	0.40
Rb	0.9	0.9	0.7	0.8	0.9	0.7	0.4	0.8	0.7	1.0	1.3	0.7	0.1	0.7	0.5	0.5	1.4	0.5	0.9	0.6	0.8	0.7	0.5	0.7	0.4
Sr	11.8		15.1	35.8	16.7	14.5	18.6		37.7		10.3	13.8		25.6	22.0		12.9		25.5	17.2	29.4	24.4	31.4	13.8	11.7
Y	0.04	0.04	0.05	0.03	0.07	0.02	0.04	0.04	0.13	0.00	0.03	0.01	0.02	0.03	0.04	0.01	0.02	0.01	0.15	0.06	0.02	0.01	0.02	0.02	0.01
Zr		0.2				0.1	0.1	0.1		0.3	0.1	0.2	0.3			0.5	0.1	0.4				0.3			0.1
Nb	0.019	0.011	0.009	0.016	0.038	0.002	0.005	0.007	0.012	0.002	0.002	0.005	0.013	0.020	0.023	0.004	0.002	0.004	0.034	0.010	0.012	0.004	0.005	0.008	0.002
Cs	1.2	0.3	0.2	0.2	0.5	0.3	0.1	0.3	0.2	0.3	0.7	0.3	0.02	0.2	0.1	0.2	0.6	0.1	0.3	0.2	0.2	0.1	0.1	0.3	0.04
Ba	1.8	1.6	1.5	4.2	1.6	1.6	1.0	1.9	3.7	1.3	3.4	1.3	0.8	1.8	1.7	3.1	5.1	1.1	1.9	1.4	7.8	15.2	1.2	1.2	3.6
La	0.002	0.021	0.003	0.008	0.003	0.001	0.003	0.010	0.002	0.010	0.005	0.006	0.020	0.002	0.005	0.010	0.008	0.010	0.005	0.003	0.003	0.005	0.004	0.001	0.001
Ce	0.017	0.042	0.006	0.017	0.008	0.003	0.007	0.022	0.005	0.021	0.009	0.011	0.041	0.005	0.010	0.021	0.015	0.023	0.010	0.005	0.005	0.010	0.009	0.002	0.004
Pr	0.001	0.005	0.001	0.002	0.001	BDL	0.001	0.002	0.000	0.002	0.001	0.001	0.005	0.000	0.001	0.002	0.002	0.002	0.001	0.001	0.001	0.001	0.001	BDL	0.001
Nd	0.002	0.014	0.003	0.009	0.003	0.001	0.003	0.007	0.001	0.006	0.004	0.004	0.017	0.001	0.004	0.006	0.006	0.007	0.005	0.002	0.001	0.004	0.003	0.001	0.001
Sm	0.001	0.001	0.001	0.001	0.001	0.001	BDL	0.001	0.001	0.000	BDL	BDL	0.003	0.001	0.000	BDL	BDL	0.001	0.002	0.001	0.001	0.001	BDL	BDL	0.001
Eu	0.001	0.001	0.001	0.001	0.001	0.001	BDL	BDL	0.001	BDL	0.001	BDL	0.001	0.001	BDL	0.001	0.001	BDL	0.001	0.001	0.003	0.003	BDL	BDL	0.001
Gd	BDL	0.002	0.002	0.002	0.001	BDL	0.001	0.001	0.003	BDL	0.001	BDL	0.003	0.001	BDL	BDL	0.001	0.001	0.006	0.003	0.000	0.001	BDL	0.001	BDL
Tb	BDL	BDL	0.001	0.000	0.000	BDL	BDL	BDL	0.001	BDL	BDL	BDL	BDL	BDL	BDL	BDL	BDL	BDL	0.001	0.001	BDL	BDL	BDL	BDL	BDL
Dy	0.001	0.005	0.004	0.002	0.001	0.001	0.002	0.003	0.010	BDL	0.002	BDL	0.004	0.001	0.000	0.001	0.001	0.001	0.011	0.005	0.001	0.001	0.001	0.001	BDL
Ho	BDL	0.002	0.001	0.000	0.000	0.000	0.001	0.001	0.004	BDL	0.001	BDL	0.002	BDL	BDL	BDL	0.001	BDL	0.003	0.002	BDL	BDL	0.001	0.001	BDL
Er	0.001	0.007	0.004	0.002	0.003	0.003	0.006	0.006	0.015	0.001	0.004	0.002	0.005	0.001	0.001	0.001	0.003	0.001	0.011	0.006	0.001	0.001	0.002	0.003	0.001
Yb	0.009	0.013	0.013	0.007	0.004	0.011	0.019	0.016	0.034	0.003	0.012	0.009	0.015	0.013	0.009	0.005	0.010	0.005	0.026	0.014	0.006	0.004	0.008	0.010	0.006
Lu	0.001	0.003	0.002	0.001	0.003	0.003	0.004	0.003	0.006	0.001	0.003	0.002	0.003	0.002	0.002	0.001	0.002	0.001	0.004	0.003	0.001	0.001	0.002	0.002	0.001
Hf	0.0007	0.0042	0.0004	0.0008	0.0022	0.0023	0.0023	0.0025	0.0006	0.0063	0.0025	0.0044	0.0067	0.0004	0.0005	0.0106	0.0022	0.0063	0.0006	0.0003	0.0004	0.0058	0.0002	0.0004	0.0028
Pb	0.019	0.008	0.036	0.001	0.017	0.001	0.023	0.022	0.023	0.012	0.018	0.008	0.017	0.016	0.005	0.005	0.009	0.021	0.003	0.015	0.005	0.108	0.006	0.008	0.010
Th	0.0006	0.0004	0.0007	0.0007	0.0015	0.0004	0.0002	0.0005	0.0007	0.0004	0.0005	0.0002	0.0009	0.0007	0.0007	0.0007	0.0002	0.0003	0.0007	0.0004	0.0007	0.0005	0.0003	0.0003	0.0007
U	0.0004	0.0003	0.0005	0.0004	0.0008	0.0007	0.0018	0.0002	0.0006	0.0012	0.0011	0.0017	0.0007	0.0042	0.0007	0.0002	0.0002	0.0009	0.0004	0.0006	0.0041	0.0008	0.0003	0.0005	0.0006
Sb	0.002	0.009	0.001	0.006	0.006	0.001	0.010	0.004	0.002	0.002	0.006	0.008	0.008	0.007	0.007	0.003	0.006	0.006	0.006	0.001	0.002	0.052	0.005	0.001	0.008

[a]All elements in ppm, except for TiO_2, in weight percent. All of the elements are presented on an anhydrous basis. See text for analytical precision. BDL, below detection limit.

Table 3b. Average

Element	Value
Li	2.7
Sc	6.8
TiO_2, wt %	0.003
V	6.6
Cr	2673
Co	98
Ni	2224
Cu	3
Zn	39
Ga	0.3
As	0.33
Rb	0.7
Sr	21.2
Y	0.04
Zr	0.2
Nb	0.01
Cs	0.2
Ba	3.2
La	0.006
Ce	0.013
Pr	0.001
Nd	0.004
Sm	0.001
Eu	0.001
Gd	0.002
Tb	0.001
Dy	0.003
Ho	0.002
Er	0.004
Yb	0.011
Lu	0.002
Hf	0.003
Pb	0.017
Th	0.001
U	0.001
Sb	0.007

offers context as to the along-strike variability of subduction-induced chemical changes in the mantle wedge.

[34] Overall, the major element compositions of our Leg 195 serpentinized peridotites are very similar to both the South Sandwich serpentinized peridotites of *Pearce et al.* [2000] and the Leg 125 suites studied by *Parkinson et al.* [1992], *Parkinson and Pearce* [1998], and *Savov et al.* [2005b]. South Sandwich samples show lower LOI, MgO, Cr, and Ni contents and higher SiO_2, Fe_2O_3, and CaO contents than our Leg 195 suite, while the Leg 125 clasts closely resemble the Leg 195 suite in Al_2O_3, Fe_2O_3, MnO, and Na_2O abundances, with slightly lower LOI, MgO, Cr, and Ni.

[35] Our South Chamorro suite also exhibits similar rare earth element patterns, at lower overall abundances, to the South Sandwich serpentinites. The rare earth element abundances and REE patterns of the South Chamorro Seamount samples are essentially identical to those analyzed from Conical Seamount [*Savov et al.*, 2005a] (Figure 9). Both suites show U-shaped REE patterns with positive Eu anomalies. Positive Eu anomalies were also detected in the relatively fresh peridotites from ODP Leg 125 studied by *Parkinson et al.* [1992] and *Parkinson and Pearce* [1998]. With the exception of Eu anomalies, Leg 195 Mariana serpentinites also show similar REE patterns to variably fluid-modified basal peridotites in the Urals, New Caledonia, Trinity, and Troodos ophiolites [*Sharma and Wasserburg*, 1996; *Bodinier and Goddard*, 2003]. This resemblance may reflect similar suprasubduction tectonic settings, and/or similar degrees of mantle-melt interaction.

[36] The systematics of the fluid-mobile elements in the ODP legs 195 and 125 serpentinized peridotite suites are very similar. Average B contents for samples from the deeper core segments at Conical Seamount [*Benton et al.*, 2001; *Savov et al.*, 2005a] and South Chamorro Seamount (this study) are 15.0 and 15.4 ppm, respectively. The general patterns of B decline with increasing core depths resemble each other, suggesting similar interactions between infiltrating seawater and pore fluids, and also similar pH variations in associated fluids [*Benton et al.*, 2001]. Boron abundances at both sites are notably lower than those recovered from the inactive fore-arc-situated Torishima Seamount (average B$\sim$27 ppm) or peridotites from the fore-arc region of the South Sandwich arc (B = 38–140 ppm (S. Tonarini, personal communication, June 2006)), where interactions with seawater at pH values lower than those of upwelling Mariana pore fluids serve to elevate B abundances. Boron contents in the Marianas serpentinized peridotites are also much lower than those seen in abyssal peridotites reported by *Bonatti et al.* [1984] or serpentinites recovered from the Vema Fracture Zone (27–88 ppm (S. Tonarini, personal communication, June 2006)).

[37] The range of Li abundances of South Chamorro Seamount serpentinized peridotites is comparable to our measurements of abyssal peridotites from various ODP drill sites: 895D (average Li equals 0.8 ppm), 897D (average Li equals 5.2 ppm) and 920D (average Li equals 2.2 ppm) [*Savov et al.*, 2005b], as well as to data from the inactive fore-arc Torishima Seamount (average Li equals 2.4 ppm). The South Chamorro Seamount serpentinites also show similar Li abundances to those reported in serpentinized peridotites from South Sandwich fore-arc region (4.5–6 ppm (L. Chan, personal communication, June 2006)), as well as those from the Southwest Indian Ridge (0.1–19.5 ppm [*Decitre et al.*, 2002]) and from the basal segments of ophiolites (average 1.3 ppm; range 0.08–4.4 ppm) [see *Scambelluri et al.*, 2004, and references therein].

[38] Both Conical and South Chamorro Seamount serpentinized peridotites have much higher arsenic than samples from the Torishima Seamount (average As equals 0.1 ppm), abyssal peridotites (average As $\approx$ 0.032 ppm (I. Savov and R. Price, unpublished AFS measurements, 2004)) or a mantle xenolith from San Carlos, Arizona (average equals 0.07 ppm) [*Savov et al.*, 2005b] (see also Figure 7c). Cs concentrations in Leg 195 samples (average equals 0.27 ppm) are higher than those from Leg 125 (average equals 0.15 ppm). The average Cs content of all Mariana fore-arc serpentinite peridotite clasts are similar to reported values for the subducting Pacific ocean crust ($\sim$0.32 ppm [*Kelley et al.*, 2003]). Rubidium is higher in Leg 195 samples than in South Sandwich fore-arc-serpentinized peridotites (average equals 0.36 ppm) or in Leg 125 (0.74 ppm versus 0.45 ppm, on average). Ba and Sr concentrations at the two Mariana fore-arc sites are similar (average Ba equals 1.6 ppm; average Sr equals 15 ppm). Excepting a few samples with extreme Sr (>100 ppm), the majority of the South Sandwich samples fall within the same range of Sr contents as the Leg 195 and Leg 125 samples. Thorium abundances are similarly low in serpentinites from all fore-arc sites, pointing to Th immobility

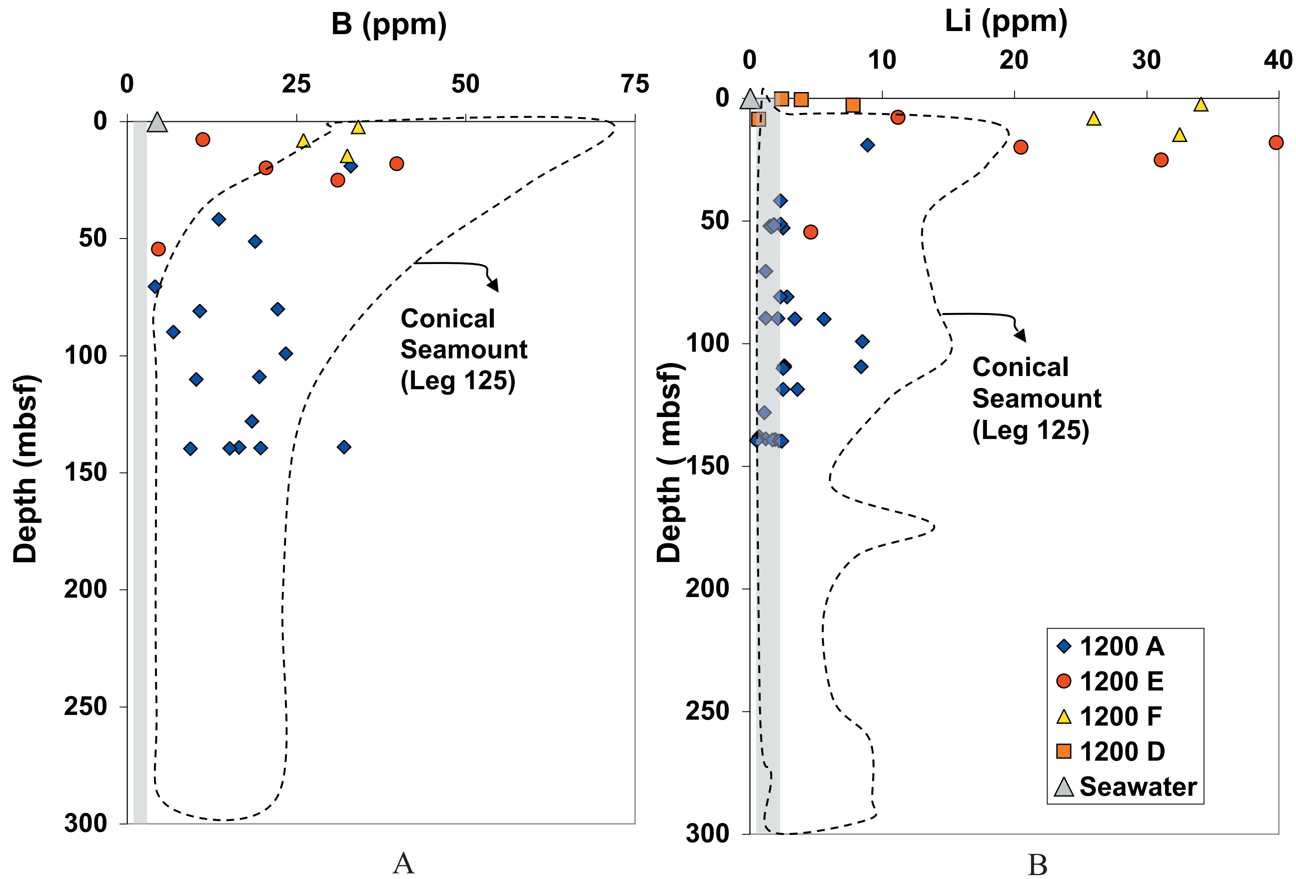

Figure 7. Elemental variations of B, Li, As, Sb, Pb, Cs, Rb, Sr, Ba, U, and Th, with increasing core depth; mbsf, meters below seafloor. (a) B in serpentinized clasts. (b) Li. (c) As (left) in Leg 195 serpentinized clasts and (right) in Leg 195 pore fluids. The abyssal serpentinite data are from of I. Savov and R. Price (unpublished AFS As measurements, 2004). (d) Sb. (e) Pb. (f) Cs. (g) Rb. (h) Sr. (i) Ba. (j) U. (k) Th. The shaded rectangular area on each plot represents the range of depleted mantle values for the elements of interest. Depleted mantle values are from *Sun and McDonough* [1989] and *Salters and Stracke* [2004]; Seawater values are from the GERM reservoir database (http://earthref.org/GERM/index.html).

during low-temperature serpentinization processes. In all Mariana fore-arc samples uranium exhibits mean concentrations and variation patterns that are up to 3 orders of magnitude lower than those reported for the South Sandwich suite (0.001 ppm versus 1.025 ppm, respectively [*Pearce et al.*, 2000]). South Chamorro Seamount lead concentrations are much lower than either those from the South Sandwich fore arc (average Pb ~ 1 ppm [*Pearce et al.*, 2000]) or from the Conical Seamount (average ~0.04 ppm). The pattern of elemental and isotopic enrichments in Mariana fore-arc serpentinites differs from that seen in abyssal serpentinites, where the reacting fluid is seawater [*Bonatti et al.*, 1984; *O'Hanley*, 1996].

7.2. Correlations Between Pore Fluid and Serpentinized Peridotite Geochemistry

[39] The pore fluids from South Chamorro and Conical seamounts are characterized by extremely high pH (approaching 12.6), high alkalinity and Na/Cl ratios, and high concentrations of sulfate, K, Rb, B, As, light hydrocarbons, and ammonia. The δ^{18}O, δD and δ^{7}Li are higher than in seawater, while chloride, Mg, Ca, Sr, Li, Si, phosphate, δ^{11}B, and ^{87}Sr/^{86}Sr ratios are lower [*Mottl*, 1992; *Benton*, 1997; *Savov et al.*, 2002; *Mottl et al.*, 2003]. With the exception of Li, which readily substitutes for Mg in olivine and pyroxenes, fresh upper mantle rocks contain infinitesimally small amounts of fluid-mobile elements, including B, As, Cs, Sb, K, Na, Rb, and Ba. Dehydration reactions within subducted ocean crust and sediments, which are significant reservoirs for these elements [*Mottl*, 1992; *Mottl et al.*, 2003; *You et al.*, 1995; *Plank and Langmuir*, 1998; *Staudigel*, 2003; *Schmidt and Poli*, 2003], release these elements into the liberated fluids. Exchanges between these fluids and the shallow mantle wedge of the Mariana fore arc lead to enrichments in both serpentinites and pore fluids in B, As, Cs, and K, as well as elevated ^{87}Sr/^{86}Sr, δ^{11}B and anomalously variable δ^{7}Li [e.g., *Benton et al.*, 2001, 2004; *Savov et al.*, 2005a, 2005b]. For a few elements (i.e., Li), high $D^{serpentine/fluid}$ values lead to abundance depletions in pore fluids, and elevated contents in serpentinized rocks. Thus, in the context of geochemical cycling, the fore-arc serpentinites and their associated upwelling pore fluids should be con-

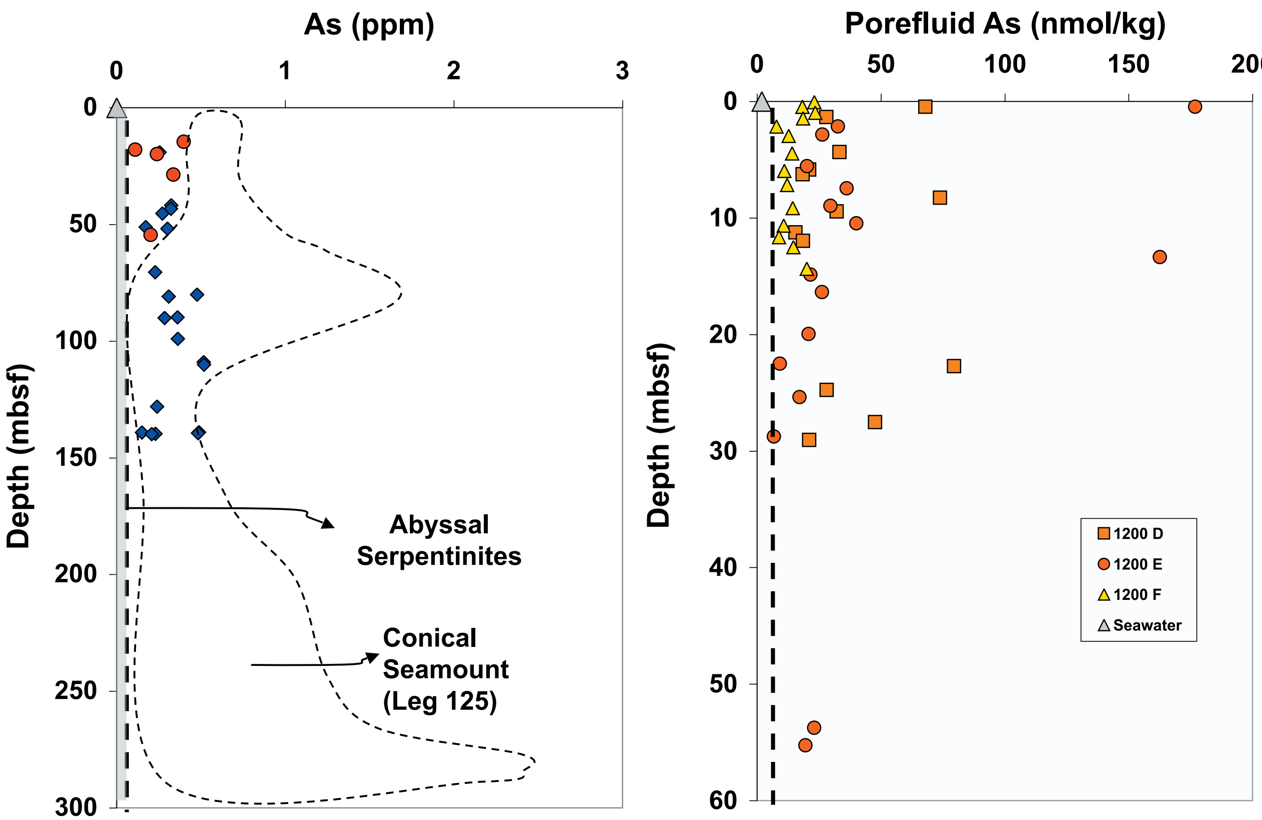

C

Figure 7. (continued)

sidered as a single subduction zone outflux inboard of the trench in the shallow fore arc.

7.3. Further Insights Into Chemical Recycling During Subduction and Impacts on Arc Magmatism

[40] As the unmodified upper mantle has a relatively simple mineralogy (olivine (OL) + OPX ± Cpx ± [spinel (Sp), plagioclase, garnet]), its incompatible trace element abundances are low to extremely low. Therefore most arc flux models presume that the anomalous trace element signatures observed in island arc lavas are derived from the sedimentary and crustal inventories of the downgoing slab, and focus on those chemical exchange processes likely to occur at the slab-mantle interface [*Plank and Langmuir*, 1993, 1998; *Elliott et al.*, 1997; *Class et al.*, 2000; *Hochstaedter et al.*, 2001; *Kelemen et al.*, 2003]. Increasing pressures, temperatures and tectonic stresses on subducting slabs, beginning in fore-arc regions, trigger prograde metamorphic changes that result in significant fluid release [*Tatsumi and Eggins*, 1995; *Schmidt and Poli*, 1998, 2003; *Hyndman and Peacock*, 2003] (Figure 12). These slab-derived fluids necessarily react with the overlying mantle wedge peridotites, creating altered ultramafic rocks that are strongly enriched in selected lithophile trace elements, but which preserve the highly depleted immobile element abundances of their protoliths. The common presumption continues to be that much of this modification takes place in the deep mantle (i.e., in a depth range consistent with communication between the slab and likely arc source regions [*Davies and Stevenson*, 1992; *Spiegelman and Kelemen*, 2003]), despite a growing body of observations from land-based studies of metamorphic massifs indicating that much of the slab fluid inventory, especially slab H_2O, is released at very shallow depths [i.e., *Iwamori*, 1998; *Bebout and Barton*, 2002; *Schmidt and Poli*, 1998, 2003; *Hyndman and Peacock*, 2003; *Scambelluri et al.*, 2004].

[41] The serpentinized muds and ultramafic clasts erupting in the Mariana fore arc provide a means to describe shallow slab outfluxes. The geochemical signatures of the Mariana fore-arc rocks mirror to a great degree the signatures in higher grade metamorphic rocks of the Catalina Schist or the Franciscan Formation "subduction complex" units, recording enrichments in elements that are depleted in these slab-derived lithologies [*Bebout*, 1995; *Bebout et al.*, 1999; *King et al.*, 2003, 2006]. The complementary elemental and isotopic homogenizations recorded in these different fore-arc suites point to a substantive and distinctive material outflux during the early stages of subduction that must be addressed in geochemical mass balance calculations for subduction systems.

[42] In classical subduction flux models [i.e., *Plank and Langmuir*, 1998],

$$
\begin{aligned}
&[\text{subduction flux(measured at arcs)}] \\
&\quad = [\text{incoming slab flux}] + [\text{erosion flux}] - [\text{underplating flux}] \\
&\qquad - [\text{accretion flux}],
\end{aligned}
$$

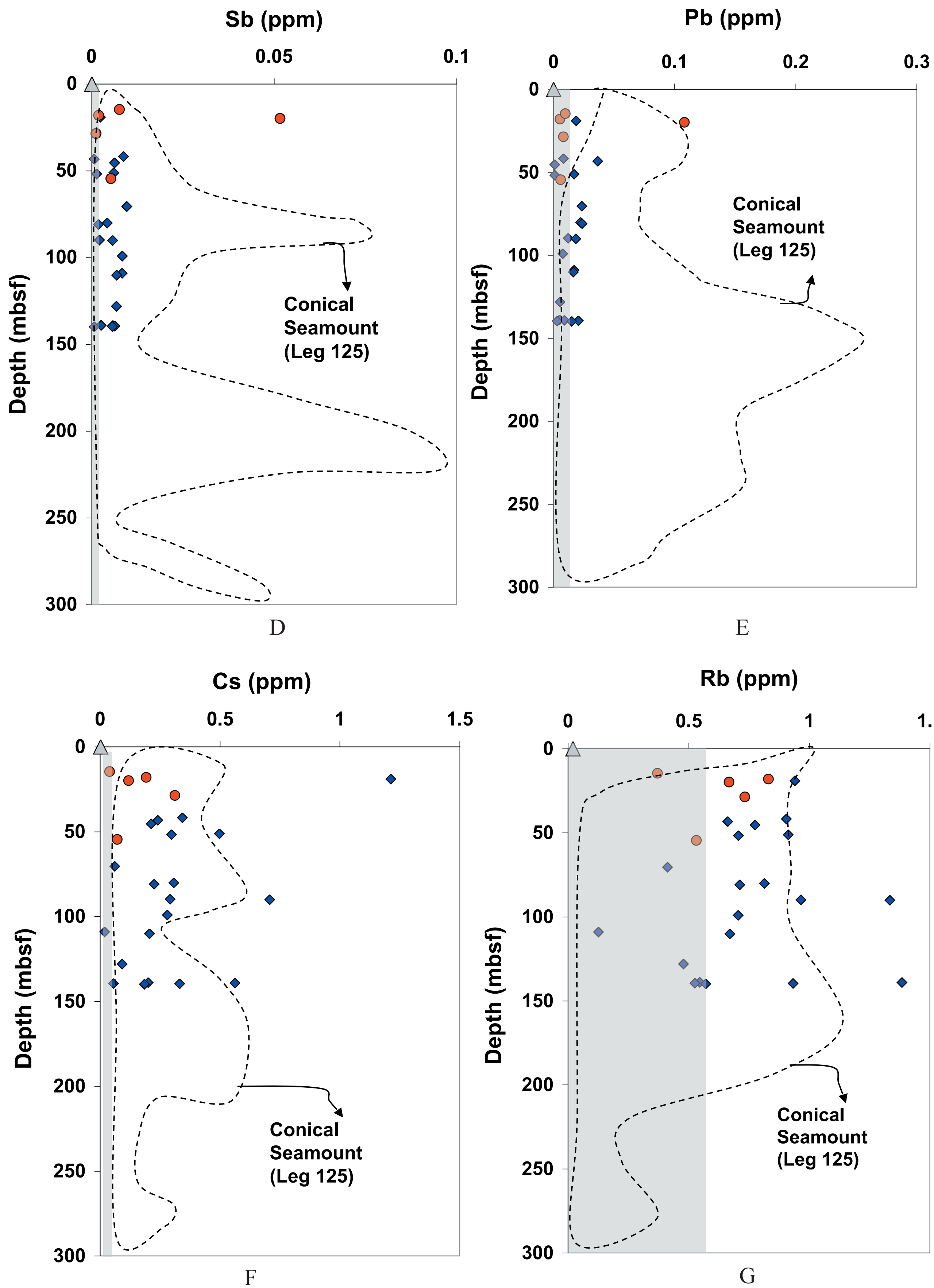

Figure 7. (continued)

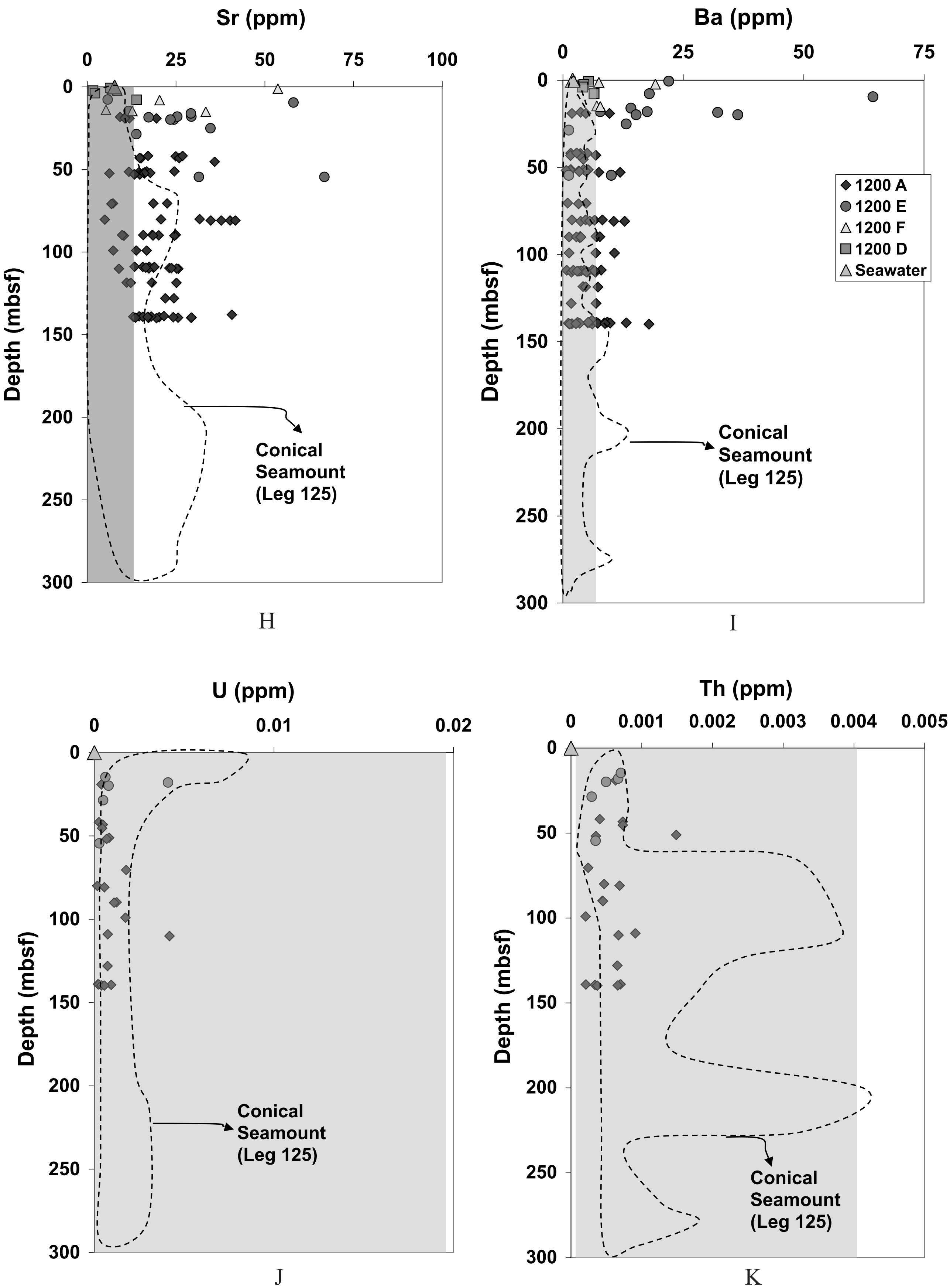

Figure 7. (continued)

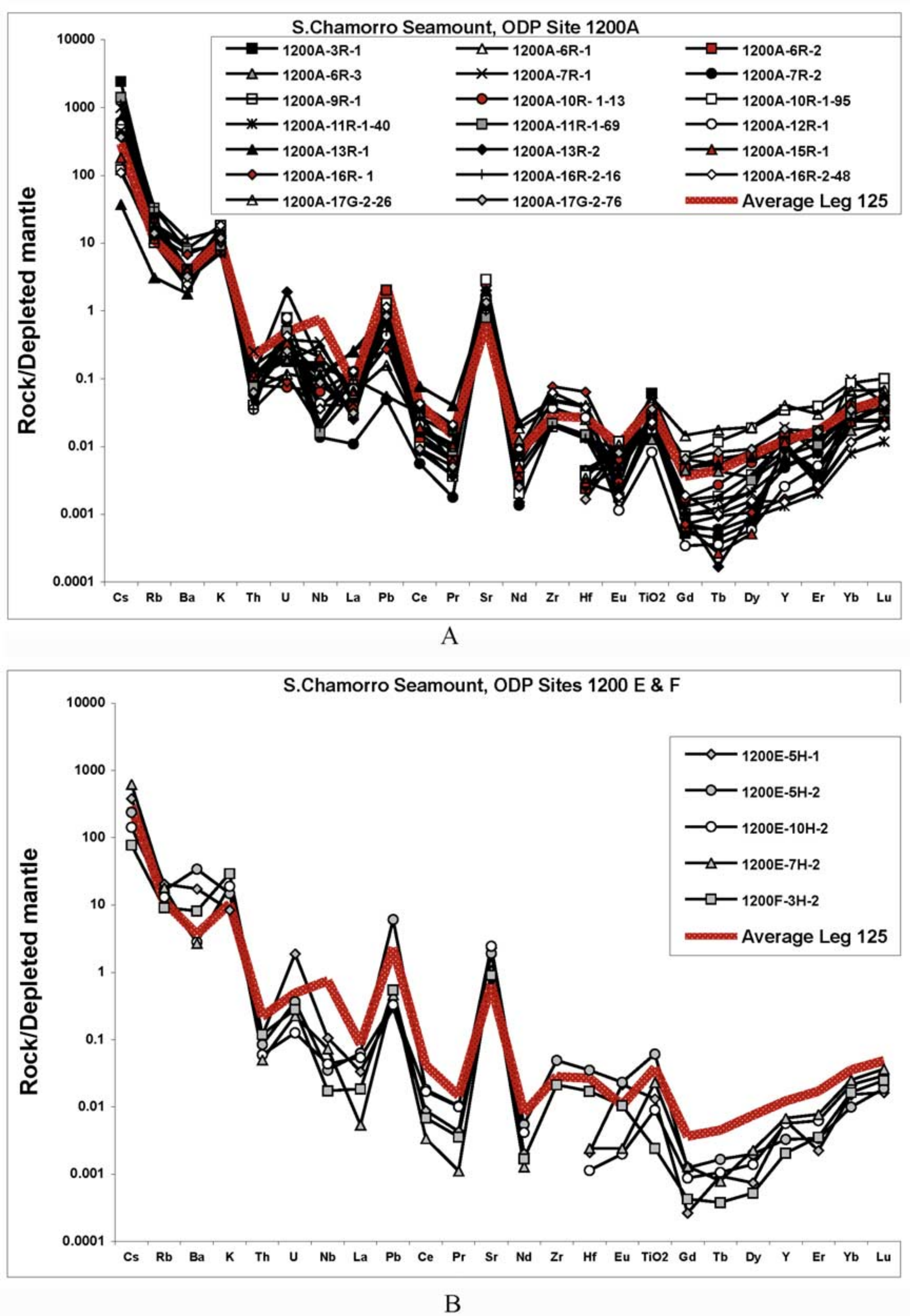
S.Chamorro Seamount, ODP Site 1200A
Rock/Depleted mantle
10000
1000
100
10
1
0.1
0.01
0.001
0.0001
1200A-3R-1
1200A-6R-1
1200A-6R-2
1200A-6R-3
1200A-7R-1
1200A-7R-2
1200A-9R-1
1200A-10R- 1-13
1200A-10R-1-95
1200A-11R-1-40
1200A-11R-1-69
1200A-12R-1
1200A-13R-1
1200A-13R-2
1200A-15R-1
1200A-16R- 1
1200A-16R-2-16
1200A-16R-2-48
1200A-17G-2-26
1200A-17G-2-76
Average Leg 125
Cs Rb Ba K Th U Nb La Pb Ce Pr Sr Nd Zr Hf Eu TiO2 Gd Tb Dy Y Er Yb Lu
A
S.Chamorro Seamount, ODP Sites 1200 E & F
Rock/Depleted mantle
10000
1000
100
10
1
0.1
0.01
0.001
0.0001
1200E-5H-1
1200E-5H-2
1200E-10H-2
1200E-7H-2
1200F-3H-2
Average Leg 125
Cs Rb Ba K Th U Nb La Pb Ce Pr Sr Nd Zr Hf Eu TiO2 Gd Tb Dy Y Er Yb Lu
B

Figure 8

with the tacit assumption that the slab influx can be considered as a single coherent influx, although a growing body of published work indicates different types of influxes from different components on the slab (i.e., fluid inputs versus melt inputs; sediment versus basalt derived [e.g., *Defant and Drummond*, 1990; *Kepezhinskas et al.*, 1996; *Elliott et al.*, 1997; *King et al.*, 2006]). Our results point to the presence of an additional elemental outflux in the fore arc, at least in the IBM subduction system, though given the magnitude of likely fluid releases at fore-arc depths, it is probable that even in settings where serpentinite mud volcanism is not observed, such an outflux may manifest itself in other ways. To specify the general flux calculations of *Plank and Langmuir* [1998] to the Marianas, we have removed the accretion flux, as accretion is not believed to occur in the Izu-Bonin-Marianas arc-basin system [*Mrozowski et al.*, 1981; *Stern et al.*, 2004] and have added a fore-arc outflux based on our combined Legs 125 and 195 serpentinite results and slab fluid release estimates beneath fore-arc regions from *Schmidt and Poli* [1998].

[43] Subtracting 10 km of fore-arc crust [*Hussong et al.*, 1981] and assuming 1000 km island arc length and 20°subduction angle, the total volume of ultramafic mantle wedge under the Mariana fore-arc region for depths between 10 and 40 km (i.e., depths of active mud volcanism and blueschist facies metamorphism) is $\sim 1.3 \times 10^{15}$ m^3. Assuming the density of peridotite to be 3.4 g/cm^3, we calculate that the mass of unserpentinized mantle in the Mariana fore arc is 4.36×10^{18} kg. The total area of the slab that is dehydrating is $\sim 85.4 \times 10^{10}$ m^2. If the slab is losing ~5.5% of its H_2O between 10 and 40 km (assuming 4–6 wt % H_2O loss, as reported for blueschists facies rocks [*Schmidt and Poli*, 2003], the mass of H_2O released into the shallow fore arc is $\sim 5 \times 10^{15}$ kg. The amount of water released every year from 1 m^2 section of the entire dehydrating portion of Pacific slabs under the Mariana fore arc (10 to 40 km depth) is $\sim 2.4 \times 10^{10}$ kg/yr [*Savov et al.*, 2005b]. Given that ~12 wt % H_2O can be hosted in serpentine (and chlorite) [*O'Hanley*, 1996; *Schmidt and Poli*, 1998, 2003], the amount of serpentine that this water can produce from fresh unaltered peridotite mantle is $\sim 2 \times 10^{10}$ kg/yr. In Tables 5a and 5b we list the results of our fore-arc slab depletion estimates for several key subduction trace elements.

[44] *Fryer and Fryer* [1987] suggested that extensive serpentinization resulting from long-term H_2O releases into the fore-arc mantle should produce a volume increase, which might explain the fore-arc rise in the IBM system, and other subduction settings globally. However, if one assumes a static, nonconvecting fore arc, >50 Ma of active subduction-related fluid release will completely hydrate the shallow portions of the mantle wedge and result in unrealistically high fore-arc uplift (~7 km). As relatively unaltered peridotites are found at both of the sampled Mariana seamounts [*Parkinson et al.*, 1992; *Parkinson and Pearce*; 1998; *Pearce et al.*, 2000; *Savov et al.*, 2005a, 2005b], it is clear that large segments of the fore-arc mantle wedge remain relatively unmodified (see Figure 12). In order for the fore-arc mantle to absorb (accommodate) the very large fluid influx ($\sim 5.8 \times 10^8$ g/m^2 of slab) without becoming entirely serpentinized, some turnover of mantle material is necessary.

[45] We suggest that serpentinized fore-arc mantle wedge is dragged downward by subduction, where it can be sampled during arc volcanism. As first noted by Y. Tatsumi and coworkers [*Tatsumi*, 1986; *Tatsumi and Eggins*, 1995], the deep burial of serpentinized fore-arc rocks can occur as frictional stresses mechanically disaggregate the slab surface and erode the mantle wedge above the décollement zone, incorporating serpentinized mantle into the aggregated subducting inventory (for discussion, see *King et al.* [2006]). This process is essentially one of subduction erosion, and it proceeds independent of mantle convection, but eventually downdragged, fore-arc-modified (serpentinized) mantle will reach deeper mantle regions (>60 km depths), where it may become convectively entrained (see Figure 12). A process like this one has been called upon to explain the observed B and B isotope systematics of fore-arc and arc rocks [*Benton et al.*, 2001; *Straub and Layne*, 2002], as well as Cl, F, and large-ion lithophile element (LILE) systematics of andesite melt inclusions from the Izu arc [*Straub and Layne*, 2003].

[46] On the basis of evidence from slab-sensitive tracers such as δ^{11}B, ^{87}Sr/^{86}Sr and Pb isotopes, the mass of serpentinized fore-arc mantle sampled in arc sources to produce the observed signatures in erupted lavas is small relative to inputs of fluids/melts from the deeper slab [*Defant and Drummond*, 1990; *Kepezhinskas et al.*, 1996; *Ishikawa and Tera*, 1999; *Hochstaedter et al.*, 2001]. However, as shown in Tables 5a and 5b, this serpentinized mantle plays a critical role in the geochemical cycles of fluid-mobile elements. The calculated elemental outfluxes at Conical and South Chamorro seamounts are all comparable within uncertainty, and several are even equal to each other (Table 5b). This indicates that the shallow slab outflux, at least in terms of these key elements, is similar along the Mariana arc, which means that prograde metamorphic reactions at both sites are releasing fluids of similar compositions.

[47] Active serpentinite mud volcanism seems to be confined, at present, to the Mariana fore arc. There may be a connection between the thin sediment veneer, the absence of an accretionary prism (characteristic for the Marianas [*Mrosowski et al.*, 1981; *Stern et al.*, 2004]) and

Figure 8. (a) Depleted mantle-normalized multielement plot of selected samples from South Chamorro Seamount, ODP Leg 195, Site 1200, Hole A. Note the large LILE, Sr, and Pb spikes and the depletions of the HFSE and REE. Also a thick solid line shows the average abundances of serpentinized peridotites recovered from Conical Seamount, ODP Leg 125 [after *Savov et al.*, 2005b]. (b) Depleted mantle-normalized multi element plot for selected samples from South Chamorro Seamount, ODP Leg 195, Site 1200, holes E and F. Note that the displayed patterns are equivalent to the one of serpentinite peridotite samples from Hole A. Also a thick line shows the average abundances of serpentinized peridotites recovered from Conical Seamount, ODP Leg 125 [after *Savov et al.*, 2005b]. Depleted mantle values are from *Sun and McDonough* [1989] and *Salters and Stracke* [2004].

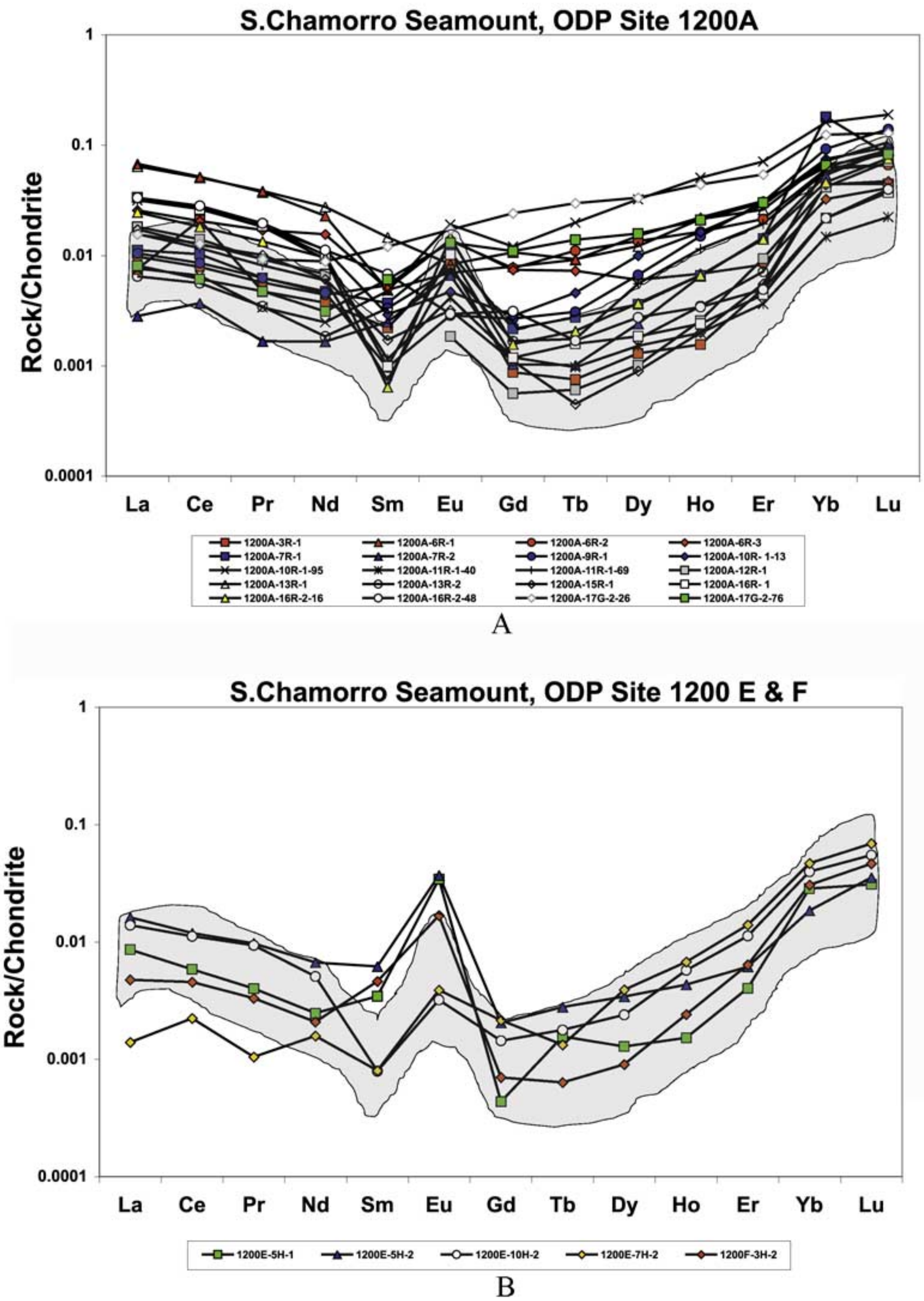

Figure 9. Coryell-Masuda diagram for selected samples from South Chamorro Seamount, ODP Leg 195, Site 1200, (a) Hole A and (b) holes E and F. Note the very low abundances, the overall U-shaped pattern, and the positive Eu anomaly. The shaded area in the background marks the range of REE in serpentinized peridotites from other fore-arc sites in the Izu-Bonin-Mariana [*Parkinson and Pearce*, 1998; *Savov et al.*, 2005a, 2005b] and the South Sandwich [*Pearce et al.*, 2000] arc-basin systems. Chondrite meteorite values are from *Nakamura* [1974].

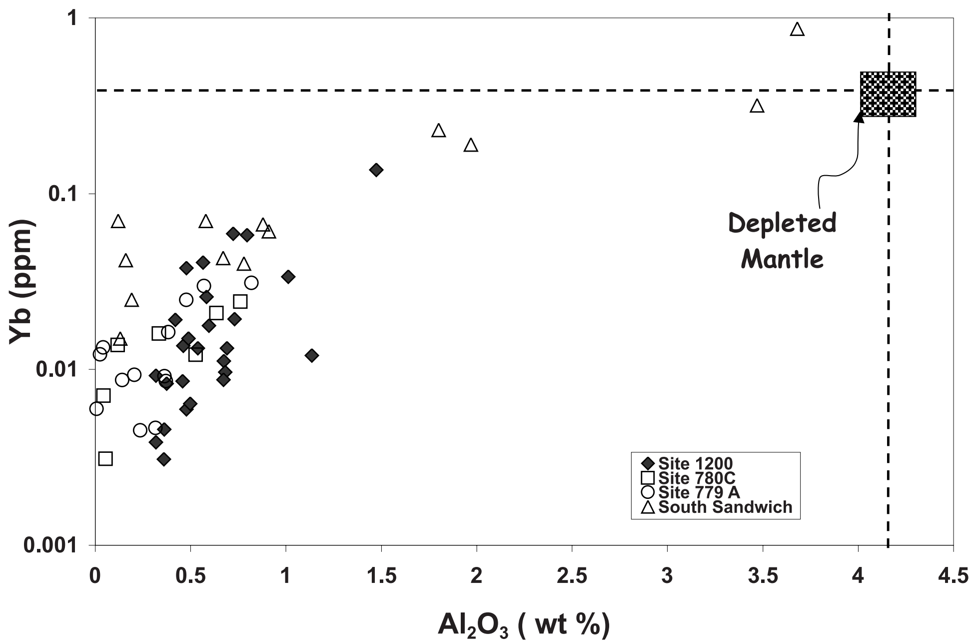

Figure 10. Al_2O_3 variation with Yb in serpentinized peridotites. Note that the vertical scale is logarithmic. Diamonds, South Chamorro Seamount, ODP Site 1200; squares, Conical Seamount; ODP Site 780C; circles, Conical Seamount; ODP Site 779A; triangles, South Sandwich peridotites [*Pearce et al.*, 2000]. Depleted mantle values are from *Bodinier and Godard* [2003] and *Salters and Stracke* [2004].

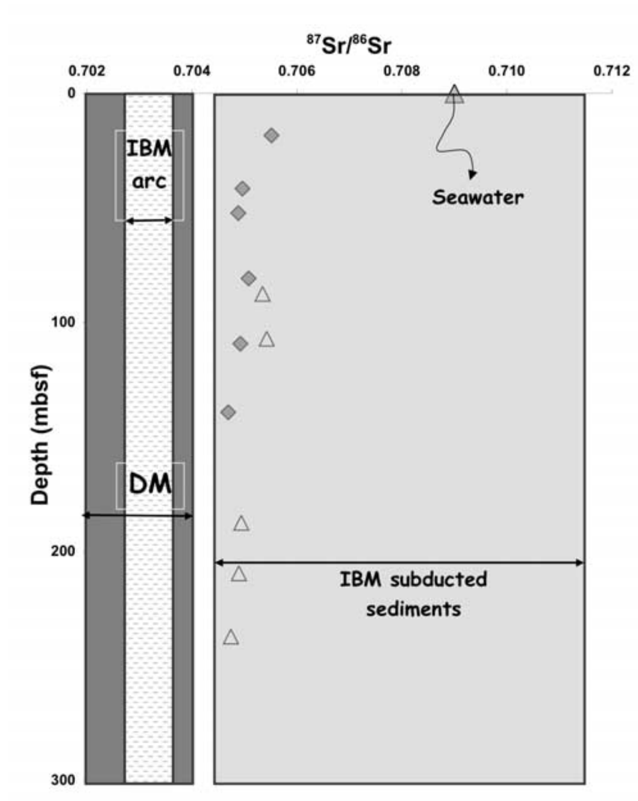

Figure 11. Variation of the $^{87}Sr/^{86}Sr$ of serpentinized peridotites from South Chamorro Seamount (diamonds) and Conical Seamount (triangles) with increasing core depth; mbsf, meters below seafloor. Seawater values are from *Haggerty and Chaudhuri* [1992]. Dark grey field indicates the $^{87}Sr/^{86}Sr$ ratios found in depleted mantle peridotites [*Salters and Stracke*, 2004]; light grey field highlights the range of $^{87}Sr/^{86}Sr$ isotope ratios of subducted IBM sediments [after *Elliott et al.*, 1997] and the field with dashed horizontal lines marks the range for the IBM arc volcanics.

Table 4. The $^{87}Sr/^{86}Sr$ Ratio of Serpentinized Peridotites From South Chamorro Seamount for Site 1200 and Hole A[a]

	Depth, mbsf					
	18.3	41.61	52.28	80.8	109.3	139.29
Core-section	3R-1	6R-1	7R-2	10R-1	13R-1	16R-2
Interval	49–52	20–23	61–67	90–93	59–61	32–35
Piece	1B	2	1C	11	7	2
Sr, ppm	19.5	26.8	16.1	34.8	16.5	17
LOI, %	15	15	12	14.5	14	13
$^{87}Sr/^{86}Sr$	0.705513	0.704962	0.704893	0.705079	0.704924	0.704688
2σ	0.000014	0.000007	0.000008	0.000008	0.000008	0.000009

[a]See text for accuracy and analytical precision.

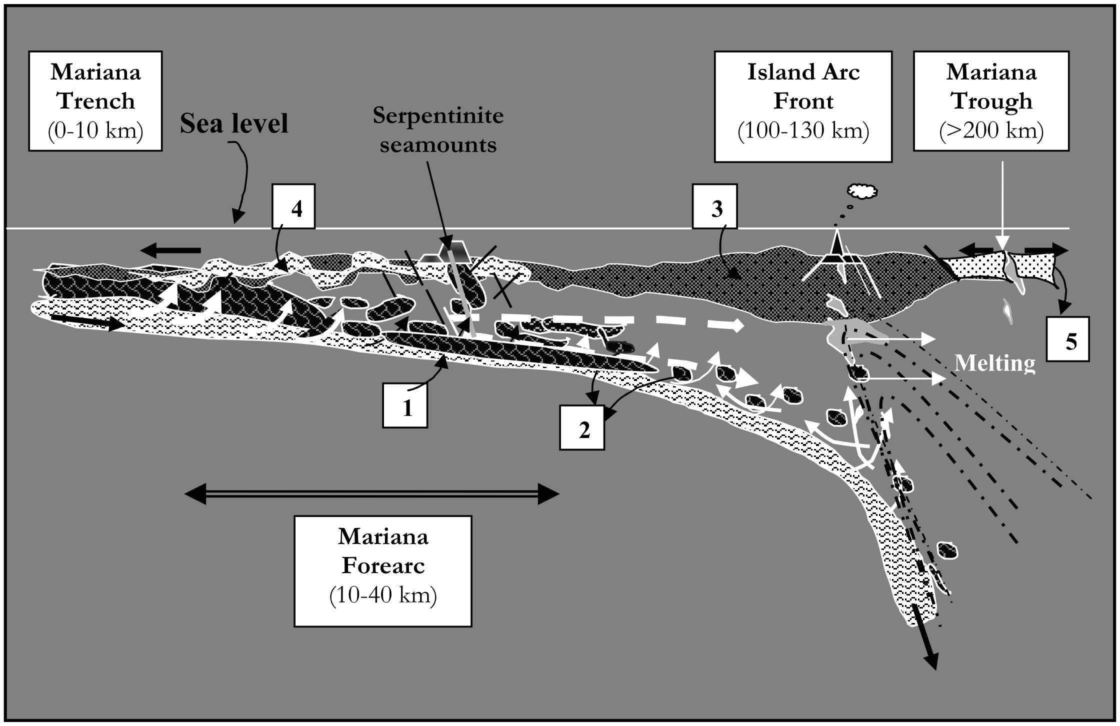

Figure 12. Cartoon illustrating a cross section through the Mariana subarc mantle wedge region discussed in the text. Note that at shallow depth to Benioff zone (0–20 km) the fore-arc mantle is entirely serpentinized. With progressive subduction the serpentinites are becoming less common, and deeper in the mantle wedge they constitute lenses (or ‘‘plums’’) within unaltered mantle peridotite rocks. However, these ‘‘plum’’-like serpentinite bodies are down-dragged to regions where mantle actively flows and thus serpentinites can reach regions where melting is achieved and thus contribute to the geochemical signatures of island arc volcanoes. 1, Altered oceanic crust and sediments; 2, Serpentinite; 3, Island arc crust; 4, fore-arc crust (or trapped preexisting seafloor); 5, back-arc crust. The white arrows size indicates fluid expelled from the subducting slab (according to the model of *Schmidt and Poli* [1998, 2003] and *Hyndman and Peacock* [2003]). The thick black arrows indicate the direction of plate motion [see *Stern et al.*, 2004, and references therein]. Note that the amount of fluid release is gradually decreasing with increasing depth of subduction and that regions of serpentinized mantle materials are dragged down to or near arc magma generation regions.

Table 5a. Parameters Used in the Mass Balance Calculations Discussed in the Text[a]

Parameter	Value
Pacific slab angle	20
Convergence rate, mm/yr	40
Length of the Mariana slab/fore-arc wedge, km	1000
Fore-arc hydrous phases, %	12
H_2O release in blueshist facies metamorphism, %	5
Length of slab needed for 100% serpentinization, km	85 400
Million years of active subduction for 100% serpentinization	21.5
Slab area under Mariana fore arc at 10–40 km depth, m^2	8.54×10^{10}
Volume of the Mariana fore arc, m^3	1.28×10^{15}
Mass of peridotite mantle, kg	4.36×10^{18}
Mass of H_2O in fore-arc mantle, kg	5×10^{16}
Mass of the serpentinized mantle, kg	6.07×10^{17}
Mass of the subducted slab [AOC+sediment], kg	1.4×10^{22}

[a]Subduction rates and Pacific slab dip angle are from *Stern et al.* [2004]; depth to the slab is from *Fryer et al.* [1992]; dehydration rates, mantle wedge mineralogy and H_2O content are from *Schmidt and Poli* [1998, 2003] and *Hyndman and Peacock* [2003]. We used the following densities: dry peridotite of 3.4 g/cm^3; altered oceanic crust (AOC) of 3.0 g/cm^3; and Mariana trench sediment of 1.86 g/cm^3 [*Plank and Langmuir*, 1998].

Table 5b. Fore-Arc and Slab Elemental Concentrations, Mass, and Calculated Outfluxes[a]

	B	Cs	As	Li	Sb	Ba	Pb	Rb	U	Th
Average Leg 195 serpentinite concentration, ppm	15	0.15	0.328	2.45	0.021	1.62	0.014	0.744	0.001	0.0006
Depleted mantle, ppm	0.05	0.00005	0.014	1.56	0.0011	0.45	0.018	0.041	0.0022	0.00593
Total available from subducted Pacific AOC, kg	6.3×10^{12}	1×10^{11}	3.45×10^{11}	1.3×10^{12}	8×10^{10}	2.5×10^{13}	4.8×10^{11}	2.4×10^{12}	4.6×10^{10}	2.1×10^{11}
Available from trench sediment, kg	5.5×10^{12}	4.14×10^{11}	1.33×10^{12}	1.5×10^{13}	3×10^{10}	2×10^{13}	5.3×10^{11}	1.2×10^{13}	3.8×10^{11}	3×10^{11}
Available on the slabs under Mariana fore arc, kg	1.2×10^{13}	5.2×10^{11}	1.68×10^{12}	1.6×10^{13}	1.1×10^{11}	4.5×10^{13}	1×10^{12}	1.5×10^{13}	4.3×10^{11}	5.1×10^{11}
Mass in the fore arc before serpentinization, kg	2.2×10^{11}	2.2×10^{9}	6.1×10^{10}	6.8×10^{12}	4.8×10^{9}	2×10^{12}	7.8×10^{10}	1.8×10^{11}	9.6×10^{9}	2.6×10^{10}
Mass of element added to the Mariana fore arc, kg	9.1×10^{12}	9.1×10^{10}	2.0×10^{11}	1.5×10^{12}	3.6×10^{9}	9.8×10^{11}	8.5×10^{9}	4.5×10^{11}	6.3×10^{8}	3.64×10^{8}
Mariana fore-arc element reservoir mass, kg	9.3×10^{12}	9.32×10^{10}	2.6×10^{11}	8.3×10^{12}	8.4×10^{9}	2.9×10^{12}	8.7×10^{10}	6.3×10^{11}	1×10^{10}	2.6×10^{10}
Mariana serpentinized fore-arc reservoir concentration, ppm	2.1	0.02	0.06	1.9	0.002	0.7	0.02	0.14	0.002	0.0006
Outflux at Leg 125 (percent depletion of the slab inventory)	77	18	12	9	3	2	1	3	2	0
Outflux at Leg 195 (percent depletion of the slab inventory)	79	32	17	9	12	3	2	2	1	0
Average fore-arc percent depletion of subducted inventory	78	25	15	9	7	3	2	2	1	0

[a]The Marianas sample lithology, geochemistry, and densities are from the following sources: Mariana Trench sediments [*Plank and Langmuir*, 1998]; AOC [*Kelley et al.*, 2003; *Staudigel*, 2003], depleted mantle [*Sun and McDonough*, 1989; *Salters and Stracke*, 2004]. We subtracted the entire volume of the fore arc between 0 and 10 km, assuming that the H_2O budgets there could be strongly affected by fluid leaving the sediment column without mineral dehydration reactions taking place, much like at accretionary prisms [*You et al.*, 1993, 1995]. Conical Seamount data are after *Savov et al.* [2000, 2005b].

the serpentinite mud volcanism. Nearly 5% of the core material recovered from the South Chamorro drill sites are metamorphosed basalts and gabbros [*Guggino et al.*, 2002; *Savov et al.*, 2005a]. The lack of abundant metasediments suggests that very little sedimentary cover may persist on the basaltic crust subducting beneath South Chamorro Seamount. This may mean that at ~30 km depths, the disaggregated remnants of ~500 m of sediments at the Mariana Trench [*Plank and Langmuir*, 1998] may already be finely mixed with subducting oceanic crust and mantle wedge peridotite. Diverse mixed lithologies are reported from various on-land mélange exposures of fore-arc materials [*Fryer et al.*, 1995, 2000; *King et al.*, 2003, 2006]. One possible consequence of the subduction of such mixed lithologies is that variable degrees of melt and fluid extraction from highly heterogeneous sources (altered ocean crust, sediments, serpentinites), may contribute to the development of mantle domains with diverse elemental and/or isotopic signatures (for the case of Li and Li isotopes, see *Benton et al.* [2004]; for the case of major and trace elements and Sr and Nd isotopes, see *King et al.* [2006]). Anomalous alkaline arc lavas, such as those erupting in the northern Seamount province of the Marianas [see *Stern et al.*, 2006], or in the Trans-Mexican Volcanic arc [*Carmichael et al.*, 1996, and references therein] may result from the melting of such mantle regions.

8. Conclusions

[48] Serpentinized peridotites from the South Chamorro Seamount record similar enrichments of fluid-mobile elements and isotopic tracers as those from the Conical Seamount, a pattern consistent with the release of H_2O-rich fluids from the subducting plate under high P/low T conditions. These slab outfluxes of FME recorded in the Mariana serpentinized peridotites show that the fore arc plays an important, if unrecognized, role in the geochemical cycle of subduction. The fore-arc "flux" and/or "reservoir" is selective, playing a role in the subduction zone budgets of relatively few elements, though for these elements (in particular B, As, Cs and Li) its importance is substantial (Tables 5a and 5b). The extreme B enrichment of the fore-arc mantle wedge (almost 80% of the slab inventory) is consistent with the inferences of cross-arc studies that little or no B is subducted past arcs [i.e., *Ryan and Langmuir*, 1993; *Ishikawa and Nakamura*, 1994; *Ryan et al.*, 1995, 1996; *Noll et al.*, 1996] and with the proposition that some small percentage of serpentinized fore-arc mantle material becomes involved in arc melting. Fore-arc enrichments of Cs, As, Li, and Sb are also substantial, although constraints on the slab inputs of chalcophile elements are still poor. This highly selective fore-arc "reservoir" carries a distinctive fingerprint, such that fore-arc contributions to subarc mantle source regions can be identified.

[49] Our understanding of the role of fore arcs in subduction zone geochemistry is incomplete because the actual fluid outfluxes associated with serpentinite generation are unknown. Studies of exposed on-land fore-arc serpentinites, such as within the Franciscan mélange in California [*Bebout et al.*, 1999; *King et al.*, 2003, 2006], may help improve our understanding of the three-dimensional structure of the serpentinite seamounts, toward quantifying the extent of

mantle-fluid interaction and thereby of shallow FME outfluxes. Given the very divergent behaviors of different trace elements in fore-arc settings, documentation of the slab sources of these shallow outfluxes (i.e., sediment- versus altered crust-derived fluids) may require an approach different from that taken in the study of arc volcanic products.

[50] **Acknowledgments.** This research was carried out as part of the senior author's Ph.D. dissertation research during the 2003–2004 JOI/USSAC Schlanger Fellowship. It was funded by JOI/USSAC Leg 195 postcruise science support grant to J.R. and I.S. I.S also acknowledges the help of Terry Plank and Katie Kelley, who allowed full access to their ICP-MS Facility at Boston University and helped with the sample preparation and data quality checks. We thank Ilenia Arienzo for her help with the Sr isotope analyses at Istituto Nazionale di Geofisica e Vulcanologia–Osservatorio Vesuviano. Nathan Becker produced the maps of South Chamorro Seamount with data collected by Fryer under grants from the National Science Foundation, OCE-9907063 and OCE0002584. Steve Guggino and Roy Price helped with the DCP-AES and AFS analysis of Li and As at USF. We appreciate the help and stimulating discussions with ODP Leg 195 Shipboard Scientific Party (especially Mike Mottl and Mette Kristensen). This paper benefited from detailed reviews and suggestions by Julian Pearce, Ian Parkinson, and Richard Arculus. We also wish to thank the following people for valuable advice, sample contribution, and/or data sharing: Sonia Tonarini, Lui Chan, Robbie King, Thomas Zack, Jim Gharib, and Jeff Alt. This research used samples and/or data provided by the Ocean Drilling Program. ODP is sponsored by the U.S. National Science Foundation (NSF) and participating countries under the management of Joint Oceanographic Institutions (JOI), Inc.

References

Bebout, G. (1995), The impact of subduction-zone metamorphism on mantle-ocean chemical cycling, *Chem. Geol.*, *126*(2), 191–218.

Bebout, G., J. G. Ryan, W. Leeman, and A. Bebout (1999), Fractionation of trace elements by subduction-zone metamorphism-effect of convergent margin thermal evolution, *Earth Planet. Sci. Lett.*, *171*(1), 63–81.

Bebout, G. E., and M. D. Barton (2002), Tectonic and metasomatic mixing in a subduction-zone melange: Insights into the geochemical evolution of the slab-mantle interface, *Chem. Geol.*, *187*, 79–106.

Beccaluva, L., G. Macciotta, C. Savelli, G. Serri, and O. Zeda (1980), Geochemistry and K/Ar ages of volcanics dredged in the Philippine Sea, Mariana, Yap Palau trenches and Parece-Vela Basin, in *The Tectonic and Geologic Evolution of Southeast Asian Seas and Islands*, *Geophys. Monogr. Ser.*, vol. 23, edited by D. E. Hayes, 247–270, AGU, Washington, D. C.

Benton, L. D. (1997), Origin and evolution of serpentine seamount fluids, Mariana and Izu-Bonin forearcs: Implications for the recycling of subducted material, Ph.D. dissertation, Univ. of Tulsa, Tulsa, Okla.

Benton, L. D., J. G. Ryan, and F. Tera (2001), Boron isotope systematics of slab fluids as inferred from a serpentine seamount, Mariana Forearc, *Earth Planet. Sci. Lett.*, *187*, 273–282.

Benton, L. D., J. G. Ryan, and I. P. Savov (2004), Lithium abundance and isotope systematics of forearc serpentinites, Conical Seamount, Mariana forearc: Insights into the mechanics of slab-mantle exchange during subduction, *Geochem. Geophys. Geosyst.*, *5*, Q08J12, doi:10.1029/2004GC000708.

Bloomer, S. H. (1983), Distribution and origin of igneous rocks from the landward slopes of the Mariana Trench: Implications for its structure and evolution, *J. Geophys. Res.*, *88*, 7411–7428.

Bodinier, J.-L., and M. Godard (2003), Orogenic, ophiolitic and abyssal peridotites, in *Treatise on Geochemistry*, vol. 2, *The Mantle and Core*, edited by R. W. Carson, pp. 103–171, Elsevier, New York.

Bonatti, E., J. R. Lawrence, and N. Mornadi (1984), Serpentinization of oceanic peridotites: Temperature dependence of mineralogy and boron content, *Earth Planet. Sci. Lett.*, *70*, 88–94.

Carmichael, I. S. E., R. A. Lange, and J. F. Luhr (1996), Quaternary minettes and associated lavas of Mascota, western México: A consequence of plate extension above a subduction-modified mantle wedge, *Contrib. Mineral. Petrol.*, *124*, 302–333.

Class, C., D. M. Miller, S. L. Goldstein, and C. H. Langmuir (2000), Distinguishing melt and fluid subduction components in Umnak Volcanics, Aleutian Arc, *Geochem. Geophys. Geosyst.*, *1*(6), doi:10.1029/1999GC000010.

D'Antonio, M., and M. B. Kristensen (2004), Serpentine and brucite of ultramafic clasts from the South Chamorro Seamount (Ocean Drilling Program Leg 195, Site 1200), Inferences for the serpentinization of the Mariana forearc mantle, *Mineral. Mag.*, *68*, 887–904.

Davies, H. J., and D. J. Stevenson (1992), Thermal model of subduction zone, *J. Geophys. Res.*, *97*, 2037–2070.

Decitre, S., E. Deloule, L. Reisberg, R. James, P. Agrinier, and C. Mével (2002), Behavior of Li and its isotopes during serpentinization of oceanic peridotites, *Geochem. Geophys. Geosyst.*, *3*(1), 1007, doi:10.1029/2001GC000178.

Defant, M. J., and M. S. Drummond (1990), Derivation of some modern arc magmas by melting of young subducted lithosphere, *Nature*, *347*, 662–665.

Dietrich, V., R. Emmermann, R. Oberhansli, and H. Puchlet (1978), Geochemistry of basaltic and gabbroic rocks from the West Mariana Basin and the Mariana Trench, *Earth Planet. Sci. Lett.*, *39*, 127–144.

Elliot, T., T. Plank, A. Zindler, W. M. White, and B. Bourdon (1997), Element transport from subducted slab to juvenile crust at the Mariana Arc, *J. Geophys. Res.*, *102*, 14,991–15,019.

Ertan, I. E., and W. P. Leeman (1999), Fluid inclusions in mantle and lower crustal xenoliths from the Simcoe Volcanic Field, Washington, *Chem. Geol.*, *154*, 83–95.

Fryer, P. (2002), Detailed structures of the Mariana forearc serpentine mud volcanoes from side-scan sonar mapping: Implications for formation of serpentinite mélange deposits, *Eos Trans. AGU*, *83*(47), Fall Meet. Suppl., Abstract T72A-1230.

Fryer, P., and G. J. Fryer (1987), Origins of nonvolcanic seamounts in a forearc environment, in *Seamounts, Islands, and Atolls*, *Geophys. Monogr. Ser.*, vol. 43, edited by B. H. Keating et al., 61–69, AGU, Washington, D. C.

Fryer, P. B., and M. H. Salisbury (2006), Leg 195 synthesis: Site 1200–Serpentinite seamounts of the Izu-Bonin/Mariana convergent plate margin (ODP Leg 125 and 195 drilling results), *Proc. Ocean Drill. Program Sci. Results* [CD-ROM], *195*.

Fryer, P., E. L. Ambos, and D. M. Hussong (1985), Origin and emplacement of Mariana Forearc seamounts, *Geology*, *13*, 774–777.

Fryer, P., et al. (1992), *Proceedings of the Ocean Drilling Program, Scientific Results*, vol. 125, Ocean Drill. Program, College Station, Tex.

Fryer, P., M. Mottl, L. Johnson, J. Haggerty, S. Phipps, and H. Maekawa (1995), Serpentine bodies in the forearcs of western Pacific convergent margins: Origin and associated fluids, in *Active Margins and Marginal Basins of the Western Pacific*, *Geophys. Monogr. Ser.*, vol. 88, edited by B. Taylor and J. Natland, pp. 259–279, AGU, Washington, D. C.

Fryer, P., C. Wheat, and M. Mottl (1999), Mariana blueschist mud volcanism: Implications for conditions within the subduction zone, *Geology*, *27*, 103–106.

Fryer, P., J. Lockwood, N. Becker, C. Todd, and S. Phipps (2000), Significance of serpentine and blueschist mud volcanism in convergent margin settings, in *Ophiolites and Oceanic Crust: New Insights from Field Studies and Ocean Drilling Program*, edited by Y. Dilek et al., *Spec. Pap. Geol. Soc. Am.*, *349*, 35–51.

Fryer, P., J. Gharib, K. Ross, I. Savov, and M. J. Mottl (2006), Variability in serpentinite mudflow mechanisms and sources: ODP drilling results on Mariana forearc seamounts, *Geochem. Geophys. Geosyst.*, *7*, Q08014, doi:10.1029/2005GC001201.

Gruau, G., J. B. Griffiths, and C. Lecuyer (1998), The origin of the U-shaped rare earth patterns in ophiolite peridotites: Assessing the role of secondary alteration and melt/rock reaction, *Geochim. Cosmochim. Acta*, *62*, 3545–3560.

Guggino, S., I. P. Savov, J. G. Ryan, and ODP Leg 195 Scientific Party (2002), Light element systematics of metamorphic clasts from ODP Legs 125 and 195, S. Chamorro and Conical seamounts, Mariana Forearc, *Eos Trans. AGU*, *83*(19), Spring Meet. Suppl., Abstract V51A-08.

Haggerty, J. A., and S. Chaudhuri (1992), Strontium isotopic composition of the interstitial waters from Leg 125: Mariana and Bonin forearcs, *Proc. Ocean Drill. Program Sci. Results*, *125*, 397–400.

Halama, R., I. P. Savov, W. F. McDonough, R. Rudnick, and J. G. Ryan (2006), Li isotope recycling: Insights from the sub-arc mantle, *Eos Trans. AGU*, *87*(52), Fall Meet. Suppl., Abstract V-34C-03.

Hochstaedter, A., J. Gill, R. Peters, P. Broughton, P. Holden, and B. Taylor (2001), Across-arc geochemical trends in the Izu-Bonin arc: Contributions from the subducting slab, *Geochem. Geophys. Geosyst.*, *2*(7), doi:10.1029/2000GC000105.

Hussong, D. M., et al. (1981), *Initial Reports of the Deep Sea Drilling Project*, vol. 60, U.S. Govt. Print. Off., Washington, D. C.

Hyndman, R. D., and S. M. Peacock (2003), Serpentinization of the forearc mantle, *Earth Planet. Sci. Lett.*, *85*, 1–16.

Ishii, T., P. T. Robinson, H. Maekawa, and R. Fiske (1992), Petrological studies of peridotites from diapiric serpentinite seamounts in the Izu-Ogasawara-Mariana forearc, Leg 125, *Proc. Ocean Drill. Program Sci. Results.*, *125*, 445–487.

Ishikawa, T., and E. Nakamura (1994), Origin of the slab component in arc lavas from across-arc variation of B and Pb isotopes, *Nature*, *370*, 205–208.

Ishikawa, T., and F. Tera (1999), Two isotopically distinct fluid components involved in the Mariana arc: Evidence from Nb/B ratios and B, Sr, Nd, and Pb isotope systematics, *Geology*, *27*, 83–86.
Iwamori, H. (1998), Transportation of H_2O and melting in subduction zone, *Earth Planet. Sci. Lett.*, *160*, 65–80.
Kelemen, P. B., K. Hanghoj, and A. R. Greene (2003), One view of the geochemistry of subduction-related magmatic arcs, with emphasis on primitive andesite and lower crust, in *Treatise on Geochemistry*, vol. 3, *The Crust*, edited by R. L. Rudnick, 593–659, Elsevier, New York.
Kelemen, P. B., et al. (2004), *Proceedings of the Ocean Drilling Program*, *Initial Reports*, vol. 209, 188 pp., Ocean Drill. Program, College Station, Tex.
Kelley, K. A., T. Plank, J. Ludden, and H. Staudigel (2003), Composition of altered oceanic crust at ODP sites 801 and 1149, *Geochem. Geophys. Geosyst.*, *4*(6), 8910, doi:10.1029/2002GC000435.
Kepezhinskas, P., M. J. Defant, and M. S. Drummond (1996), Progressive enrichment of island arc mantle by melt-peridotite interaction inferred from Kamchatka xenoliths, *Geochim. Cosmochim. Acta*, *60*, 1217–1229.
King, R. L., M. Kohn, and J. Eiler (2003), Constraints on the petrologic structure of the subduction zone slab-mantle interface from Franciscan Complex exotic ultramafic blocks, *Geol. Soc. Am. Bull.*, *115*(9), 1097–1109.
King, R. L., G. E. Bebout, T. Moriguti, and E. Nakamura (2006), Elemental mixing systematics and Sr–Nd isotope geochemistry of mélange formation: Obstacles to identification of fluid sources to arc volcanics, *Earth Planet. Sci. Lett.*, *246*(3–4), 288–304.
Leeman, W. P. (1996), Boron and other fluid-mobile elements in volcanic arc lavas: Implications for subduction processes, in *Subduction Top to Bottom*, *Geophys. Monogr. Ser.*, vol. 96, edited by G. E. Bebout et al., pp. 269–276, AGU, Washington, D. C.
Leeman, W. P., J. F. Lewis, R. C. Evarts, R. M. Conrey, and M. J. Streck (2005), Petrologic constraints on the thermal structure of the Cascades arc, *J. Volcanol. Geotherm. Res.*, *140*, 67–105.
Lockwood, J. P. (1972), Possible mechanisms for the emplacement of alpine-type serpentinite, *Mem. Geol. Soc. Am.*, *132*, 273–287.
Luhr, J. F., and J. J. Aranda-Gómez (1997), Mexican peridotite xenoliths and tectonic terranes: Correlations among vent location, texture, temperature, pressure, and oxygen fugacity, *J. Petrol.*, *38*, 1075–1112.
Maury, R. C., M. Defant, and J.-L. Joron (1992), Metasomatism of the sub-arc mantle inferred from trace elements in Philippine xenoliths, *Nature*, *360*, 661–663.
Morris, J. D., and J. G. Ryan (2003), Subduction zone processes and implications for changing composition of the Upper and Lower Mantle, in *Treatise on Geochemistry,* vol. 2, *The Mantle and Core*, edited by R. W. Carson, pp. 451–471, Elsevier, New York.
Mottl, M. J. (1992), Pore waters from serpentine seamounts in the Mariana and Izu–Bonin Forearcs, Leg 125: Evidence for volatiles from the subducting slab, *Proc. Ocean Drill. Program Sci. Results*, *125*, 373–385.
Mottl, M. J., S. C. Komor, P. Fryer, and C. L. Moyer (2003), Deep-slab fluids fuel extremophilic Archaea on a Mariana forearc serpentinite mud volcano: Ocean Drilling Program Leg 195, *Geochem. Geophys. Geosyst.*, *4*(11), 9009, doi:10.1029/2003GC000588.
Mrosowski, C. E., D. E. Hayes, and B. Tylor (1981), Multichannel seismic reflection surveys of Leg 60 sites, *Initial Rep. Deep Sea Drill. Proj.*, *60*, 709–731.
Nakamura, N. (1974), Determination of REE, Ba, Fe, Mg, Na and K in carbonaceous and ordinary chondrites, *Geochim. Cosmochim. Acta*, *38*, 757–775.
Niu, Y., and R. Hékinian (1997), Basaltic liquids and harzburgitic residues in the Garrett Transform: A case study at fast spreading ridges, *Earth Planet. Sci. Lett.*, *146*, 243–258.
Noll, P. D., H. E. Newsom, W. P. Leeman, and J. G. Ryan (1996), The role of hydrothermal fluids in the production of subduction zone magmas: Evidence from siderophile and chalcophile trace elements and boron, *Geochim. Cosmochim. Acta*, *60*, 587–611.
O'Hanley, D. (1996), *Serpentinites: Records of Tectonic and Petrological History*, 271 pp., Oxford Univ. Press, New York.
Parkinson, I. J., and R. J. Arculus (1999), The redox state of subduction zones: Insights from arc-peridotites, *Chem. Geol.*, *160*, 409–423.
Parkinson, I. J., and J. A. Pearce (1998), Peridotites from the Izu-Bonin-Mariana forearc (ODP Leg 125), Evidence for mantle melting and melt-mantle interaction in a supra-subduction zone setting, *J. Petrol.*, *39*, 1577–1618.
Parkinson, I. J., J. A. Pearce, M. F. Thirlwall, K. T. M. Johnson, and G. Ingram (1992), Trace element geochemistry of peridotites from the Izu-Bonin- Mariana forearc, Leg 125, *Proc. Ocean Drill. Program Sci. Results*, *125*, 487–507.
Parkinson, I. J., R. J. Arculus, and S. M. Eggins (2004), Peridotite xenoliths from Grenada, Lesser Antilles Island Arc, *Contrib. Mineral. Petrol.*, *146*, 241–262.
Pearce, J. A., P. D. Kempton, G. M. Nowell, and S. R. Noble (1999), Hf-Nd element and isotope perspective on the nature and providence of mantle and subduction components in western Pacific arc-basin systems, *J. Petrol.*, *40*, 1579–1611.
Pearce, J. A., P. F. Baker, S. J. Edwards, I. J. Parkinson, and P. T. Leat (2000), Geochemistry and tectonic significance of peridotites from the South Sandwich arc-basin system, South Atlantic, *Contrib. Mineral. Petrol.*, *139*, 36–53.
Peate, D. W., and J. A. Pearce (1998), Causes of spatial compositional variations in Mariana arc lavas: Trace element evidence, *Island Arc*, *7*, 479–495.
Plank, T., and C. H. Langmuir (1993), Tracing trace element from sediment input to volcanic output at subduction zones, *Nature*, *362*, 739–742.
Plank, T., and C. H. Langmuir (1998), The chemical composition of subducted sediment and its consequences for the crust and mantle, *Chem. Geol.*, *145*, 325–394.
Ryan, J. G., and C. H. Langmuir (1987), The systematics of lithium abundances in young volcanic rocks, *Geochim. Cosmochim. Acta*, *51*, 1727–1741.
Ryan, J. G., and C. H. Langmuir (1993), The systematics of boron abundances in young volcanic rocks, *Geochim. Cosmochim. Acta*, *57*, 1489–1498.
Ryan, J. G., J. Morris, F. Tera, W. P. Leeman, and A. Tsvetkov (1995), Cross-arc geochemical variations in the Kurile Arc as a function of slab depth, *Science*, *270*, 625–627.
Ryan, J. G., J. Morris, G. E. Bebout, and W. P. Leeman (1996), Describing chemical fluxes in subduction zones; insights from 'depth-profiling' studies of arc and forearc rocks, in *Subduction Top to Bottom*, *Geophys. Monogr. Ser.*, vol. 96, edited by G. E. Bebout et al., pp. 263–268, AGU, Washington, D. C.
Salisbury, M. H., M. Shinohara, C. Richter, et al. (2002), *Proceedings of the Ocean Drilling Program, Initial Reports* [CD-ROM], vol. 195, Ocean Drilling Program, Texas A&M Univ., College Station.
Salters, V. J. M., and A. Stracke (2004), Composition of the depleted mantle, *Geochem. Geophys. Geosyst.*, *5*, Q05B07, doi:10.1029/2003GC000597.
Savov, I. P., J. G. Ryan, P. Mattie, and J. Schijf (2000), Fluid-mobile element systematics of ultramafic xenoliths from the Izu- Bonin- Mariana forearc: Implications for the chemical cycling in subduction zones, *Eos Trans. AGU*, *81*(48), Fall Meet. Suppl., Abstract V-21C-02.
Savov, I. P., J. G. Ryan, L. Chan, M. D'Antonio, M. Mottl, and P. Fryer (2002), Geochemistry of serpentinites from the S. Chamorro Seamount, ODP Leg 195, Site 1200, Mariana forearc- implications for recycling at subduction zones, *Geochim. Cosmochim. Geosyst.*, *66*, Abstract A670.
Savov, I. P., S. Guggino, J. G. Ryan, P. Fryer, and M. Mottl (2005a), Geochemistry of serpentinite muds and metamorphic rocks from the Mariana forearc, ODP sites 1200 and 778–779, South Chamorro and Conical seamounts, *Proc. Ocean Drill. Program Sci. Results* [Online], *195*. (Available at http://www-odp.tamu.edu/publications/195_SR/103/103.htm)
Savov, I. P., J. G. Ryan, M. D'Antonio, K. Kelley, and P. Mattie (2005b), Geochemistry of serpentinized peridotites from the Mariana Forearc Conical Seamount, ODP Leg 125: Implications for the elemental recycling at subduction zones, *Geochem. Geophys. Geosyst.*, *6*, Q04J15, doi:10.1029/2004GC000777.
Savov, I. P., D. Rost, E. Vicenzi, and T. Zack (2006), Microscale mapping of boron and lithium in the Mariana sub-arc mantle via ToF-SIMS, *Eos Trans. AGU*, *87*(36), Jt. Assem. Suppl., Abstract V43A-02.
Scambelluri, M., O. Müntener, L. Ottolini, T. Pettke, and R. Vannucci (2004), The fate of B, Cl and Li in the subducted oceanic mantle and in the antigorite breakdown fluids, *Earth Planet. Sci. Lett.*, *222*(1), 217–234.
Schmidt, M. W., and S. Poli (1998), Experimentally based water budgets for dehydrating slabs and consequences for arc magma generation, *Earth Planet. Sci. Lett.*, *163*, 361–379.
Schmidt, M. W., and S. Poli (2003), Generation of mobile components during subduction of oceanic crust, in *Treatise on Geochemistry*, vol. 3, *The Crust*, edited by R. L. Rudnick, pp. 567–593, Elsevier, New York.
Sharma, M., and G. J. Wasserburg (1996), The neodymium isotopic compositions and rare earth patterns in highly depleted ultramafic rocks, *Geochim. Cosmochim. Acta*, *60*, 4537–4550.
Spiegelman, M., and P. B. Kelemen (2003), Extreme chemical variability as a consequence of channelized melt transport, *Geochem. Geophys. Geosyst.*, *4*(7), 1055, doi:10.1029/2002GC000336.
Staudigel, H. (2003), Hydrothermal alteration processes in the oceanic crust, in *Treatise on Geochemistry*, vol. 3, *The Crust*, edited by R. L. Rudnick, pp. 511–535, Elsevier, New York.
Stern, R. J., M. J. Fouch, and S. Klemperer (2004), An overview of the Izu-Bonin Mariana subduction factory, in *Inside the Subduction Factory*,

Geophys. Monogr. Ser., vol. 138, edited by J. Eiler, pp. 175–223, AGU, Washington, D. C.

Stern, R. J., E. Kohut, S. H. Bloomer, M. Leybourne, M. Fouch, and J. Vervoort (2006), Subduction factory processes beneath the Guguan cross-chain, Mariana Arc: No role for sediments, are serpentinites important?, *Contrib. Mineral. Petrol.*, *151*, 202–221.

Straub, S. M., and G. D. Layne (2002), The systematics of boron isotopes in Izu arc front volcanic rocks, *Earth Planet. Sci. Lett.*, *198*, 25–39.

Straub, S. M., and G. D. Layne (2003), Decoupling of fluids and fluid-mobile elements during shallow subduction: Evidence from halogen-rich andesite melt inclusions from the Izu arc volcanic front, *Geochem. Geophys. Geosyst.*, *4*(7), 9004, doi:10.1029/2002GC000349.

Sun, S. S., and W. F. McDonough (1989), Chemical and isotopic systematics of oceanic basalts: Implications for mantle composition and processes, in *Magmatism in the Ocean Basins*, edited by A. S. Sounders and M. J. Norrey, *Geol. Soc. Publ.*, *42*, 313–346.

Tatsumi, Y. (1986), Formation of the volcanic front in subduction zones, *Geophys. Res. Lett.*, *13*, 717–720.

Tatsumi, Y., and S. Eggins (1995), *Subduction Zone Magmatism*, 211 pp., Blackwell, Malden, Mass.

Walter, M. J. (2003), Melt extraction and compositional variability in mantle lithosphere, in *Treatise on Geochemistry,* vol. 2, *The Mantle and Core*, edited by R. W. Carson, 363–394, Elsevier, New York.

Wessel, J., P. Fryer, P. Wessel, and B. Taylor (1994), Extension in the northern Mariana forearc, *J. Geophys. Res.*, *99*, 15,181–15,203.

Woodhead, J. D., S. Eggins, and J. A. Gamble (1993), High field strength and transition element systematics in island arc and back-arc basin basalts: Evidence for multi- phase melt extraction and a depleted mantle wedge, *Earth Planet. Sci. Lett.*, *114*, 491–504.

You, C.-F., A. J. Spivack, J. H. Smith, and J. M. Gieskes (1993), Mobilization of boron in convergent margins: Implications for the boron geochemical cycle, *Geology*, *21*, 207–210.

You, C.-F., L. Chan, A. J. Spivack, and J. M. Gieskes (1995), Lithium, boron, and their isotopes in sediments and pore waters of Ocean Drilling Program Site 808, Nankai Trough: Implications for fluid expulsion in accretionary prisms, *Geology*, *23*, 37–40.

Zack, T., I. P. Savov, and J. G. Ryan (2004), Storage of light elements in the forearc mantle wedge: SIMS measurements of serpentinites from ODP Leg 195, paper presented at International Geological Congress, Int. Union of Geol. Sci., Florence, Italy.

M. D'Antonio, Dipartimento di Scienze della Terra, Università degli Studi di Napoli Federico II, L.go S. Marcellino 10, I-80138 Naples, Italy.

P. Fryer, Hawai'i Institute of Geophysics and Planetology, University of Hawaii at Manoa, 2525 Correa Road, Honolulu, HI 96822, USA.

J. G. Ryan, Geology Department, University of South Florida, 4202 East Fowler Avenue, Tampa, FL 33620, USA.

I. P. Savov, Department of Terrestrial Magnetism, Carnegie Institution of Washington, 5241 Broad Branch Road, N.W., Washington, DC 20015-1305, USA. (savov@dtm.ciw.edu)